Wireless Power Transfer Control System and Magnetic Design

by

Ramin Rahmat Samii

A thesis submitted in partial fulfillment of the requirements for the degree of

Master of Science

in

Energy Systems

Department of Electrical and Computer Engineering
University of Alberta

ABSTRACT

In this thesis, the design and implementation of power converter and controller for wireless power transfer systems are studied. Transferring electricity without a direct use of conductors to transfer power from the source to the load has become a hot topic recently despite the existing limits on the level of transferred power, distance, and efficiency of the system. The newly commercially available fast high-power switches have enabled power electronics designers to address some of the limitations, as high frequency switching is one of the requirements for wireless power transfer. As the increase of switching frequency entails higher switching losses, soft switching methods are normally used to in transfer systems.

A new control method is introduced that guarantees the soft switching with controllable active load power injection using only one feedback. In this control method, zero voltage switching is achieved using variable frequency control. Moreover, a systematic magnetic design process is introduced to effectively design the inductive power system. The implemented magnetic design is verified with accurate Maxwell simulation. Through first harmonic approximation, a converter design is developed for the IPT system. With many uncertainties in the design process, the experimental and simulation results are slightly different. In addition, a resonant wireless power transfer system is designed through optimized searching of the available options. The bottleneck for design is identified through comprehensive analytic and simulation analyses.

ACKNOWLEDGEMENT

TABLE OF CONTENTS

LIST OF TABLES

LIST OF FIGURES

CHAPTER 1

INTRODUCTION

1.1   Background

The idea of transferring electricity without wire is almost as old as the idea of electricity for public. Although the electrical energy was cleaner than its mechanical form, the electrical engineers' ambitions were set even higher from the very beginning. In 1904, Nikola Tesla tried to make the idea of free electricity for all without any wire, through Tesla tower [1]. Although the huge project was not a success, the simple idea behind it was simple and meaningful: to pick up the magnetic energy.

Although during the next decades wireless communication was coined, Tesla's ambitious idea to transfer a large amount of power to cover a town's need was not anything close to reality for almost a century. With the introduction of semiconductor devices and their improvement in every aspect including voltage, current and frequency rating, Tesla's dream looks closer to feasibility today than any time before. With the improvement of power electronic converter technology, the AC source that Tesla dreamed has become a reality already. Meanwhile, the idea of picking up magnetic energy has found different applications after the deregulation of economy in the many countries, in contrast with Tesla's super socialist idea of free electricity for all.

Wireless power transfer (WPT) refers to a wide range of technologies, in which electric energy is transferred from a source to a load without direct use of conductors to

transfer power from the source to the load. Depending on the amount and distance of power to be transmitted, numerous methods and technologies have been developed. With the enhancement of power electronics in recent decades, some of the untouchable wireless power technologies have been realized, especially since 2007, when a research group at MIT introduced the magnetic induction resonant WPT [2].

1.2 Categorization and principle of operation

In this section, different types of technologies existing of WPT with a wide range capability are introduced and then operation principle of two important types of WPT technologies are explained. At the end, the performance evaluation parameters for WPT systems are introduced.

1.2.1 Categorization

Based on the physical functioning, WPT technologies are divided into four major categories: electromagnetic radiation, electric induction, magnetic induction and capacitive power transfer as shown in Figure 1-1.
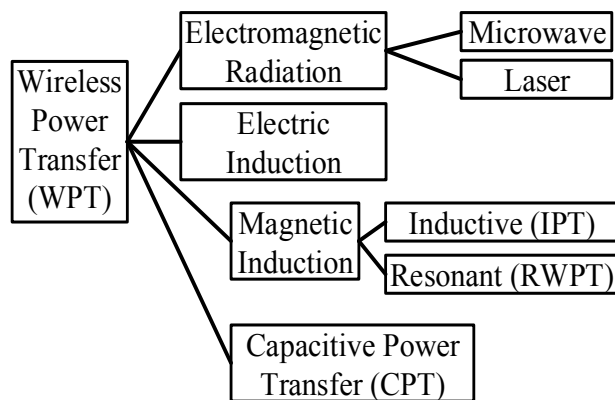
Figure 1-1: Categorization of WPT

Electromagnetic radiation works well in the far-field range [3] and is itself categorized into two types: microwave WPT and laser WPT. Microwave technology is

used in applications like supplying a sensor from far range using antennas and also RFID[1] technology [4]. Laser WPT is also a far-field function which has applications in photo-transceivers [5] and also high-altitude powered platforms [6].

For electric induction type, the power is transferred through electric field of components such as capacitors. The work range of electric induction is always in the near-field range, which means the dimensions of transmitters and receivers are bigger than the distance transferred [7].

Capacitive power transfer (CPT) refers to wireless power transfer using electric flux as the means of transfer [8]. CPT's applications are limited to short distances (millimeter range) [8].

In magnetic induction wireless power transfer (MIWPT), which is also a near-field range technology, the power is transferred using the magnetic coupling of two or more coils [9]. Based on the essence of this coupling, it is divided into two types: inductive wireless power transfer (IWPT[2] or IPT) and resonant wireless power transfer (RWPT)[3]. IWPT's applications can be found in a wide range, namely automatic guided vehicles, battery charging for people movers, electric buses and cellphone chargers [10]. Since realizing inductive coupling is limited to a short distance, the distance of IWPT for the power to be transferred is very short. Figure 1-2 shows a Murata IWPT block diagram[11]. Basics of RWPT technology was introduced by Tesla a century ago. However, RWPT was not effectively realized until recently, when 60 Watts of power was transferred through a

---

[1] Radio-frequency identification
[2] Also referred to as IPT in many references.
[3] The literature is not consistent with these terms. There are many instances (usually short-range power transfers) that resonance is, but the technology is simply referred as IPT. At these instances, it's usually the short-range essence of the work that makes the distinction.

2-metre range [2]. Although one categorization [3] mentions RWPT as near-range[4] WPT, some other references [9] consider it mid-range as the dimension of the coils in RWPT can be much smaller than the distance between the coils. Some applications of this technology are hybrid vehicles battery charging [12], robot arms [13] and also home appliances [9]. The mechanism of RWPT coupling is different from that of IWPT. In RWPT, each coil has a capacitor (either parasitic or separate), which resonate with the resonant frequency. Hence, these coils are referred to as resonators[14].
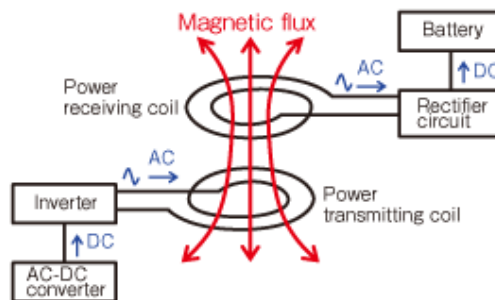
Figure 1-2: IWPT: Magnetic field display [11]

1.2.2 IWPT principle of operation

The principle of operation of IWPT is basically the magnetic current induction of one coil onto another coil [15]. As shown in Figure 1-3, the sending coil is connected to a voltage source and hence a current passes through it. The current in the coil generates a magnetic field around the coil. Any other coil in the range of this magnetic field can be induced with a current through it. This principle of operation is the same as that of transformers, with the difference that the magnetic field in transformers passed through high-permeability medium, and hence faces less reluctance. In IWPT, the medium is only air which is not a good medium for magnetic field.

---

[4] In [3], any non-radiative WPT technology is considered a near-range one.

A schematic of a typical IWPT system is shown in Figure 1-3. The two DC power supply units (DC PSUs) are plugged to AC grid. The power amplifier (PA) guarantee the amount of power to be transferred with an internal load-matching unit. The sending (transmitter) coil and the receiver coil are tagged as TX and RX respectively. The load can be either AC or DC, and that is why the diode bridge rectifier at the secondary can be removed.
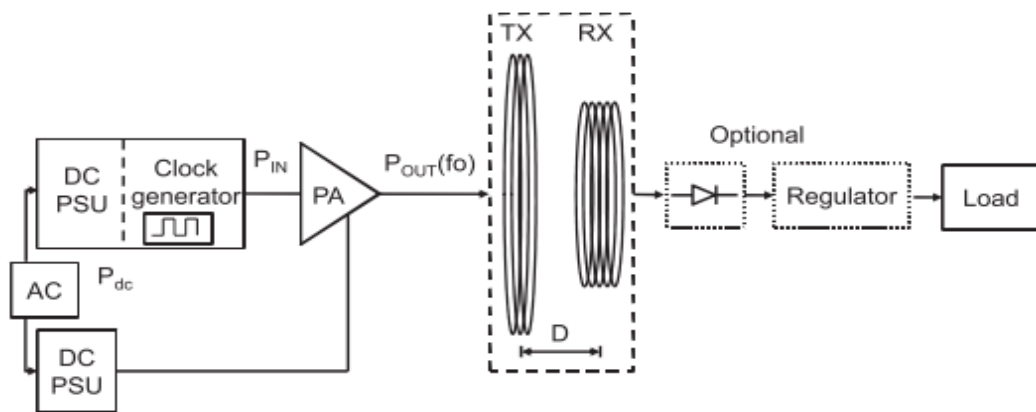
Figure 1-3: IWPT: a schematic of the system implementation [15].

Another example of IPT is introduced by [16] as shown in Figure 1-5. The coils in this structure are 70 cm and are large enough to transfer 2kW to the electric vehicle battery. The design of secondary side converter (pick-up converter) and also magnetic design of the coils is studied in [16]. The leakage inductances of the transmitter and receiver are compensated with parallel capacitors C_1 and C_2. The frequency range for the converters, which are controlled with switches on both sides, is 10-40 kHz.

The different designs for IPT focus on magnetic design and converter design. In higher operating frequencies switching loss will be noticeable. So, the lack of soft switching achievement for the aforementioned structures in [7]-[16] is an existing problem to be solved.
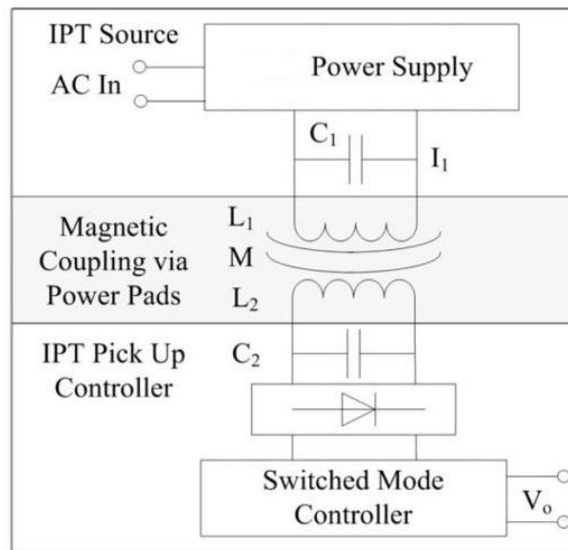
Figure 1-4: An IPT design for electric vehicles [16].

1.2.3   RWPT principle of operation

To achieve better efficiency from magnetic fields to farther distances, the concept of resonance was adopted into the magnetic induction. This idea, like most of the other WPT technologies, was developed by Tesla [17]; but it was not realized because of technical issues like power electronic devices capable of operating in such high frequencies.

The resonance in RWPT works as a continuous transaction between magnetic energy and electric energy in the coils, so that the efficiency in RWPT is higher than IWPT and hence it can achieve longer distances compared to IWPT. Figure 1-5 shows a schematic view of a typical RWPT system. From the structural viewpoint, there are two types of RWPT: one composing of the two coils, referred to as two-coil or direct RWPT system; and the other the four-coil or indirect RWPT system [14]. The four-coil system has advantages over the two coil system in terms of efficiency and maximum power transfer capability [9] in power engineering applications.

6

There are two main technical issues associated with RWPT system: one is the frequency of the input source, and the other is the high electric field in the capacitor. In Figure 1-5, the capacitors in the transmitter and receiver coils are parasitic; hence, the resonance frequency of each resonator is high in the range of several kilohertz to a few megahertz. With all the progress in power electronic devices, operation in this range is yet not realized for power applications. However, a breakthrough is expected in near future with widespread use of Gallium-nitride base switches [18].
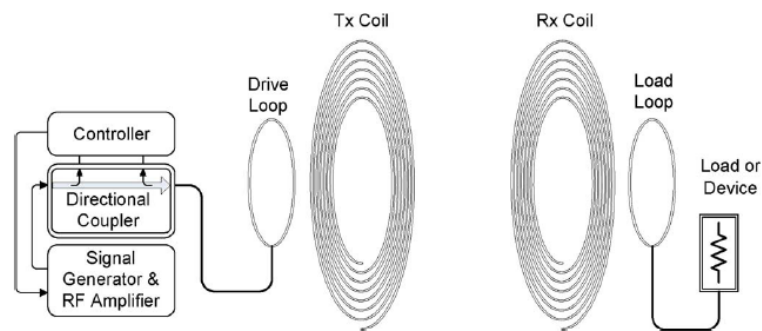
Figure 1-5: RWPT: Sketch of the magnetically coupled resonant wireless power system consisting of an RF amplifier, on the left, capable of measuring the forward and reflected powers. A two-element transmitter, made of a single-turn drive loop and high-Q coil, wirelessly powers the receiver on the right [19]

Figure 1-6 (a) and (b) show the electrical circuit models for the two-coil and four-coil RWPT systems respectively.

The two-coil schematic models two coils with their mutual inductance and two capacitors as compensators, where the four-coil schematic shows a wireless power system where additional coils are used between the source and load and is proved to increase the power transfer distance and efficiencies. There are more degrees of freedom in the four-coil model, but the design is more complicated, because of increase in the number of elements.
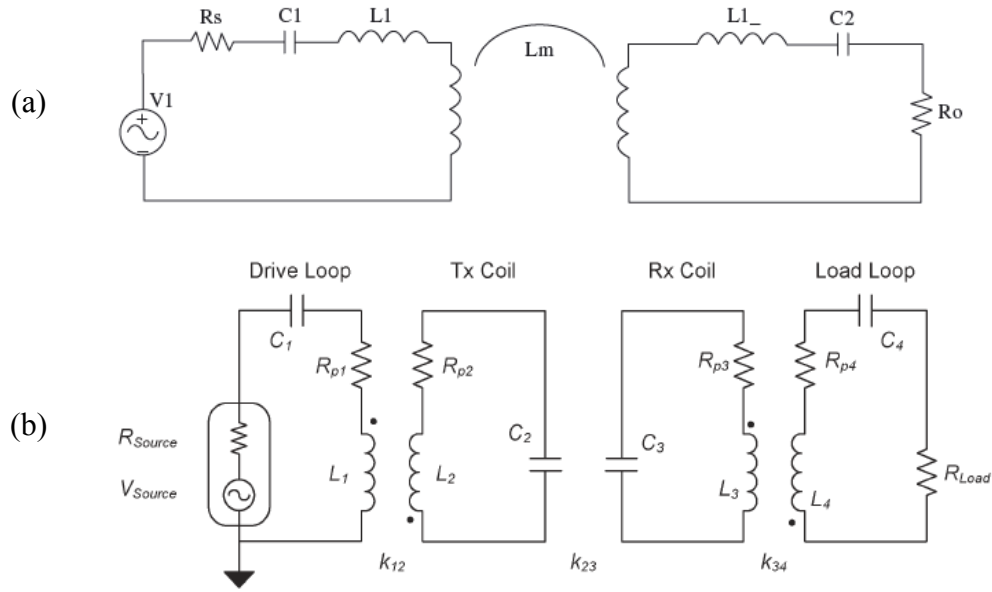
Figure 1-6: RWPT circuit model: (a) two-coil system model assuming ideal resistance-less coils; (b) four-coil system

Performance evaluation

The performance of the IWPT and RWPT systems can be evaluated by the achievable efficiency and the distance between the main transmitter and receiver coils.

In terms of efficiency, there are two parameters used to identify system performance: the wave voltage ratio denoting the output voltage to input voltage[5] of the coils, modeled as a two-port network; and power efficiency, which is the ratio of the output power to the input power[6].

In terms of power transfer distance, two important points should be discussed: 1) the maximum distance, and 2) robustness of the system with respect to the change of frequency. In applications such as charging a hybrid vehicle in static mode, the system

_____

[5] This parameter is mostly used in electronics applications, like supplying a sensor wirelessly, in the range of mill Watts.
[6] Some references [9] also mention the ratio of output power to the power after the source. In other words, the power dissipated in the voltage source is not considered as efficiency loss.

maximum distance is important [12], whereas in charging the same car while moving the robustness factor is of great importance; the reason is that the system should work in a wide range, as the car moves along the sources of power.

In this section, the mechanism of WPT technology was briefly explained. The next section is specifically about the power electronic converters used in technologies.

1.3   Converters in WPT

1.3.1   Inductive power transfer

Inductive power transfer has been applied to some power engineering applications, specifically battery charging for vehicles [20]-[21]. The advantages of transferring power wirelessly are highlighted in damp and untidy areas, where using wires can cause safety issues [22].

Class E converter is a type of resonant converter used for IPT coils due to the low harmonic distortion [23]. Class E converters' principle of operation is explained in [24]. An example of Class-E converters applied along with resonant converters is introduced in [25], the schematic of which is shown in Figure 1-7. The series (C_s) and external capacitors (C_{Ex} and C_{Ex2}) resonate and the load side voltage is controlled only with a diode.
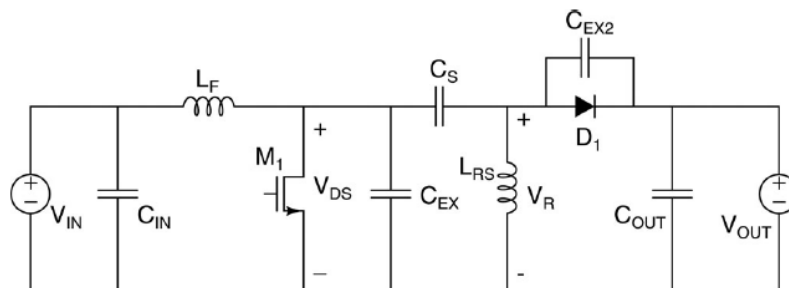
Figure 1-7: A resonant single-ended primary inductor converter introduced in [25]

As shown in Figure 1-7, C_s and L_{RS} produce the resonance frequency, while C_{EX2} along with D1 play the role of class E converters, which is to produce a ripple free DC output [25].

Another example of using power electronics in IWPT technology is introduced in [10], in which a switched mode regulator is introduced for the receiving side of the IWPT system. The analysis on the circulating current control is also provided. Figure 1-8 shows the circuit of the receiving side of the system.
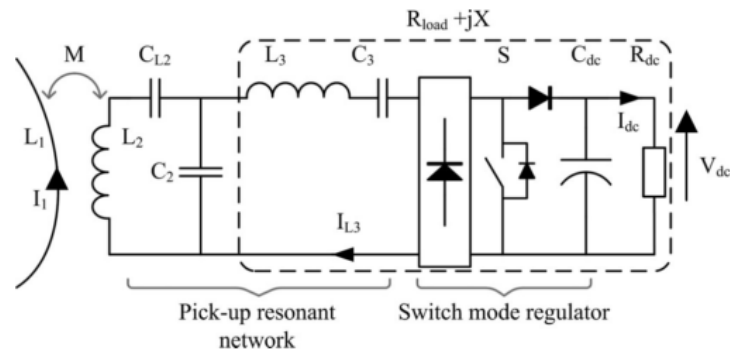
Figure 1-8: The LCL pick-up circuit for the secondary side of IWPT [7]

The term "pick-up" in this circuit refers to the receiving essence of the whole circuit. The current I_1 is the current in the transmitter coil and M is the mutual inductance between the sending and receiving coil. The authors show that this system can control the flow of power by sensing the output voltage [10].

A direct AC-AC converter is designed for the primary side of IPT converter [26]. The schematic is shown in Figure 1-9. In this method, series resonance is applied and R_{eq} can be replace by the coils and load of an IPT system. The novelty of the circuit [26] is that it does not need any DC power supply unit.
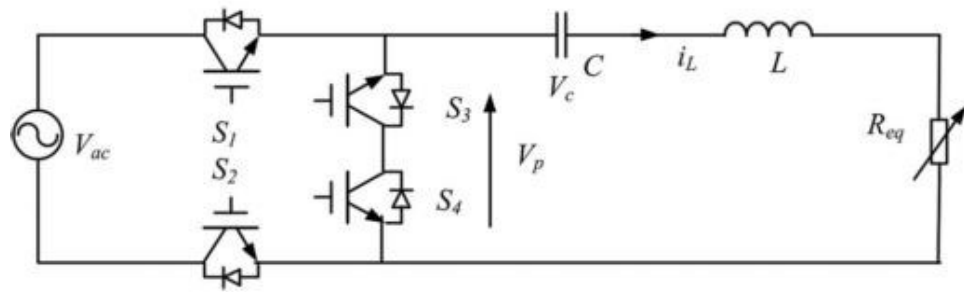
Figure 1-9: Primary side converter for IWPT [26]

A three-phase version of IPT converter was introduced in [21]. Figure 1-10 shows the schematic for a three-phase IPT converter. The primary side is controlled by full bridge converter, while the tracks at the secondary are 13-meter long, 1-meter wide coils. The vehicles can move in tracks A, B or C. However, current imbalance is a big issue for three-phase converter and necessitates the use of capacitors and wires at the secondary to achieve balanced currents.
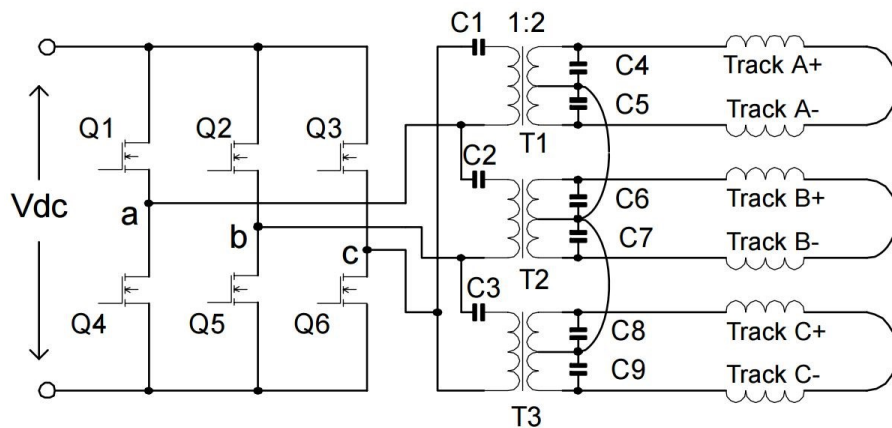
Figure 1-10: Schematic for a three-phase IWPT [21]

1.3.2   Resonant WPT

While there are numerous publications on IWPT converters, only few has been published on RWPT converters. One reason may be the older history of IWPT and more

commercialized items existing in the market. Among the numerous patents of Witricity, only one is devoted to converters [27]. To achieve smaller systems, higher frequencies operation is a necessity in WPT converters. In this regard, resonant converters are currently one of the best options for high frequency production [28]. The principle of operation of three half-bridge resonant converters is explained in [29]. Figure 1-11 shows a series half-bridge resonant converter, in which C_p is the parallel resonance role-player and $C_s/2$ is the series resonance role-player. Compared with half-bridge parallel resonant converter, half-bridge resonant converter circuit shows good voltage regulation characteristics as well as no load voltage characteristics.
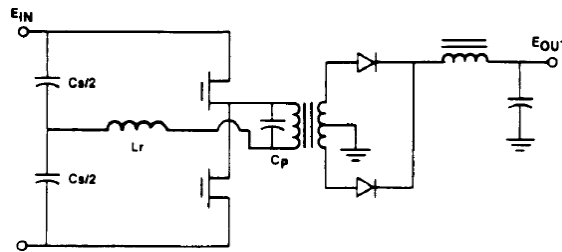
Figure 1-11: Half-bridge series-parallel loaded converter [29]

One important problem for RWPT systems to be applied to power applications, is the very high resonant frequency (larger than 50 kHz) needed. As suggested in [3] this problem can be tackled by increasing the turns ratio and the diameter of the transmitter and receiver coils. It is shown that there is a trade-off between the dimension of the RWPT system and the frequency choice of the system.

An example of the switched-mode power converters applied to RWPT systems is the one introduced in [30]. It is analogous to the work in [10] in the sense that both regulate the output voltage by applying switching in the receiving side. The left circuit in Figure 1-12: Conventional and proposed receiver circuits for RWPT [29] shows the

conventional rectifier in the receiver side of the RWPT system, and the circuit at the right shows the switched mode system to regulate the output voltage.

The efficiency and regulation characteristics of the receiver side of the RWPT system is improved compared with the uncontrolled circuit.

The EV charger proposed in [28] uses self-resonant PWM. This work has claimed efficiencies around 80% for a 6.6 KW charging interface for a distance of 12-20 cm. One of the advantage of this topology is that it does not need a second stage chopper. An alternative way is to use variable frequency to maintain the efficiency, however, due to the disadvantages of variable frequency, the authors in [31] use a fixed frequency. Another feature of the proposed topology is the bidirectional power flow, i.e. the battery can discharge and inject power to the source when needed. Figure 1-13(a) shows the schematic of the proposed system in [28], with L_s representing the transmitter and receiver coils. Figure 1-13(b) and Figure 1-13(c) show the control scheme and the equivalent ac circuit of the system respectively. This converter is controlled with constant frequency PWM with reasonable efficiency around 90%. However, the implementation is complicated with 8 controlled switches and three feedback signals.

Figure 1-12: Conventional and proposed receiver circuits for RWPT [29]

The EV charger proposed in [28] uses self-resonant PWM. This work has claimed efficiencies around 80% for a 6.6 KW charging interface for a distance of 12-20 cm. One

of the advantage of this topology is that it does not need a second stage chopper. An alternative way is to use variable frequency to maintain the efficiency, however, due to the disadvantages of variable frequency, the authors in [31] use a fixed frequency. Another feature of the proposed topology is the bidirectional power flow, i.e. the battery can discharge and inject power to the source when needed. Figure 1-13(a) shows the schematic of the proposed system in [28], with L_s representing the transmitter and receiver coils. Figure 1-13(b) and Figure 1-13(c) show the control scheme and the equivalent ac circuit of the system respectively. This converter is controlled with constant frequency PWM with reasonable efficiency around 90%. However, the implementation is complicated with 8 controlled switches and three feedback signals.

(a)

(b)

(c)

Figure 1-13: The schematic of the bidirectional converter (a), the control schemes (b) and the equivalent ac model (c) proposed in [31].

1.4   Magnetic design

IPT is still categorized as emerging technology, because of existing technical challenges such as the level of transferred power, distance range of transfer and efficiency. Unlike resonant converters, in IPT topology normally consists of two capacitors to compensate the reactive power flowing through the coils which in turn reduces the loss [32]. Among different possible resonant converter resonant tank topologies, LCL tank is the closest match for IPT applications topologies[33]. Magnetic design for resonant needs great expertise due to the importance of the magnitude of the magnetizing inductor in the model for operation in the resonant frequency. However, transformer design in wireless power is even more complicated due to the trade-off between best efficiency in specific frequency and acceptable operation in a range [34]. An acceptable design approach is used in [35] to transfer power using the current source characteristic of capacitor compensation, which is called Boucherot current source.

For the sake of saving space and weight, the coils designed for wireless power are flat spirals rather than helixes in ordinary inductors. There are three designs that are more popular, circular spiral shown in Figure 1-14, rectangular spiral shown in Figure 1-15, and DDQ shown in Figure 1-16.
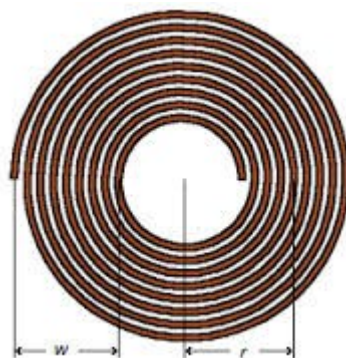
Figure 1-14**:** Circular spiral [36]
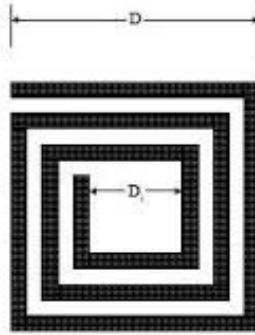
Figure 1-15: Rectangular spiral [37]

The focus in [38] is on rectangular spirals. Spiral shapes can be divided into several rectangles and mutual inductance integrals can be applied to calculate the leakage and mutual inductances [36]. There are specific analytical calculations for rectangular spirals considering the width and thickness of the track [38]. Also, there are suggestions that rectangular spiral implementation is easier than circular spiral implementation [38].

In a comparison based on mutual inductance, it is shown that circular coils offer better coupling than square coils under perfect alignment [39]. However under any misalignment, square coils are superior [39].

Several advantages are sought by adding a primary coil which is electrically in parallel to the first coil, to make multiple primary coils [40]. Multiple primary coils reduces the system sensitivity to both system components' variation such as the changes in capacitor and inductor values from the rectifier model as well as load variation[40]. As shown in Figure 1-16, using three charger pads (DDQ structure) is a more efficient, yet more complicated method to improve the spirals. The DDQ coils are more robust to misalignment and the charging zone increase compared to simpler spiral coils. The disadvantage of DDQ files is the higher amount of copper used and the non-flat structure.

Currently there are quite a few commercially available converters for hybrid electric vehicle battery charging. One example is shown in Figure 1-17 that is used in electric vehicles in France and New Zealand [12]. The advantage of this type of charging is a high level of safety in case of a failure in the charger system, due to the electric isolation between the charger and car's electric system. The magnetic design used in this approach is DDQ that shows great robustness to misalignment of the pickup coil.
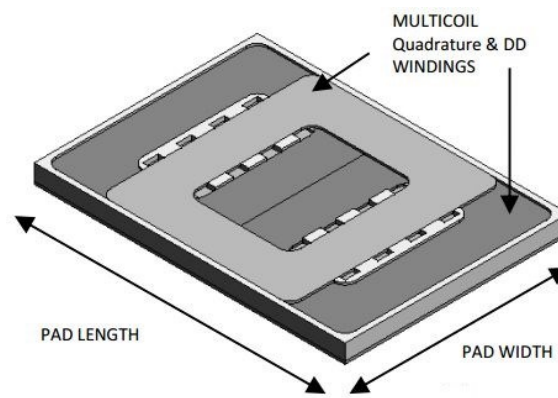
Figure 1-16: DDQ structure[41]

Currently there are quite a few commercially available converters for hybrid electric vehicle battery charging. One example is shown in Figure 1-17 that is used in electric vehicles in France and New Zealand [12]. The advantage of this type of charging is a high level of safety in case of a failure in the charger system, due to the electric isolation between the charger and car's electric system. The magnetic design used in this approach is DDQ that shows great robustness to misalignment of the pickup coil.

Normally, rectangular spiral is used for IPT technology, to use the space optimally and circular spiral is used for RWPT technology due to better use of the surface (getting higher coupling for a given surface area). The magnetic designs used in this thesis is coreless structures to avoid extra weight for the setup.
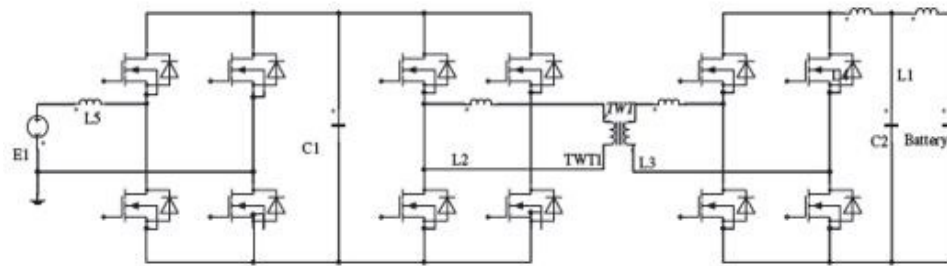
Figure 1-17: A typical inductive charger for hybrid vehicles [12]

1.5   Control methods

Among important issues in IPT converters are design and implementation of the switching strategy and control systems. It is shown that for IPT applications frequency control is one of the best approaches [42]. There is a trade-off in switching frequency selection of the IPT system. The closer the system operates to resonant frequency, the higher the efficiency is [43]. However, the frequency should be controlled so that soft switching is guaranteed for all operating conditions [41]. Using nonlinear control, soft-switching can be achieved with self-sustained methods [44]-[45]. In this thesis, a simple alterative control approach is introduced which guarantees the soft-switching with a more transparent control system block diagram. In the proposed approach in this thesis both active and reactive power injected to the wireless power system can be independently controlled. The amount of reactive power is shown to have close relationship with soft switching and efficiency of the system. This control method is not limited to IPT and can be applied to other types of converters as well. The control method that is proposed for this thesis has two objectives (transferred power and zero voltage switching) and uses only one feedback (primary side current), which makes it practically efficient.

1.6   Description of the proposed structures

Both prototypes of IPT and RWPT are studied in this thesis as shown in Figure 1-18 and Figure 1-19. Review of the existing designs reveals that it is inevitable to have inductive elements as well as capacitors which resonate in high frequency. The need for high frequency input necessitates a converter block of very fast FETS.

The block diagram of the proposed structure of IPT of Chapter 2 is shown in Figure 1-18. Capacitors are used to compensate the effect of leakage inductance to increase the efficiency. The variable distance transformer consists of two coils and is the main part of transferring power without wire (this is the wireless part of the system, where energy is delivered through air).
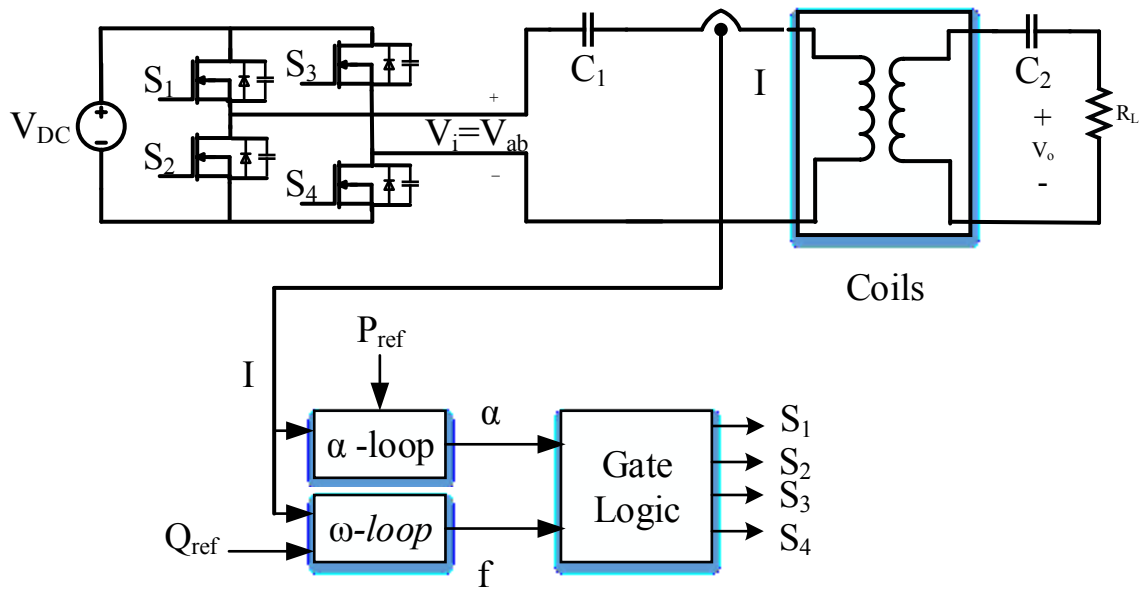
Figure 1-18: IPT scheme and its control scheme

A full bridge converter is used to generate an AC voltage at the primary of the transformer with variable frequency.

The control method for this converter is designed so that soft switching is guaranteed for a wide range of operating conditions. The feedback for the control system is the primary current and consists of two loops. The inputs of the control system is reference active and reactive powers. The proposed control method in Chapter 2 guarantees soft switching for the converter in high frequency, which is a privilege over the existing methods.

The magnetic design Figure 1-18 comprises of two coils so that magnetic energy is delivered. In the load side, the energy is received in the form of electric energy.

The control loop is supposed to trace reference power (P_{ref}), so a loop (α-loop) is designed to make sure that desired power is delivered. A second input is used to set the phase difference of voltage and current so that the switching loss is minimized in high frequency.

The IPT prototype is studied in two chapters. Chapter 2 discusses the converter part and its logic, and chapter 3 discusses the magnetic design.

In Chapter 4, an RWPT design procedure is proposed based on the output power level for a four-coil system. The structure of the coils in this design uses four coils to match the load with designed loops and coils. It is shown that unlike IPT structure, the maximum transferred power is not delivered at the shortest distance and the bottleneck for this design is the output power at the longest distance.

1.7   Objectives and scope

One of the objectives of this thesis was to develop and implement a magnetic design process for wirelessly power transfer applications. Moreover, it was intended to develop and implement a control method that is robust for wireless power application with

guaranteed soft switching of all switches. The scope of this study is focused on power engineering applications, with a minimum level of tens of Watts and not through beams of electromagnetic waves.
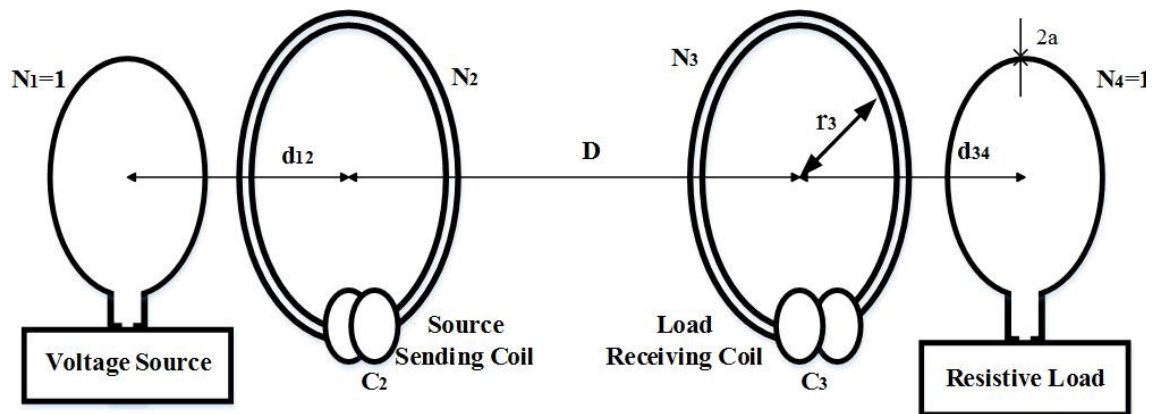
Figure 1-19: RWPT scheme

1.8   Thesis layout

In this chapter, a short literature of technologies, converters and magnetic designs related to WPT were provided. In chapter 2, a new control method is introduced for IPT wireless power system. In chapter 3, the magnetic design process is explained for the IPT system discussed in chapter 2, a case study is simulated, implemented and experimental results are provided to validate the design process. Chapter 4 provides a design methodology for four-coil RWPT configuration. Chapter 5 is dedicated to conclusion and suggested future work.

CHAPTER 2

IPT CONVERTER

2.1   Introduction

Chapter 2 and chapter 3 are devoted to the analysis of a two coil inductive wireless power transfer system. As Tesla desired a century ago, the basic need for transferring power and realizing resonance, is to have a reliable high frequency ac source which is affected least by its load. Power electronics switches have made this desire feasible through power converters. A full-bridge converter is introduced in this chapter to achieve this goal. A control method based on power feedback is introduced to achieve both soft switching and output power control.

2.2   IPT compensation types

Resonance between capacitors and inductances leads to compensation of the inductive characteristic of the circuit. In two coil systems, there are four main types of compensation based on the position of capacitor in primary and secondary [46]. In Figure 2-1 to Figure 2-4, the input voltage source (V_i), represents the model of the full bridge converter to produce ac voltage.

2.2.1   Series-series (SS)

SS systems are the most common type of compensation [41], with two capacitors in series to compensate the effect of leakage inductance of either side as shown in Figure 2-1. The dashed box in Figure 2-1 shows the coils modeled as conventional

transformer model. The advantage of series compensation is the option of directly compensating the leakage inductances of the coils.
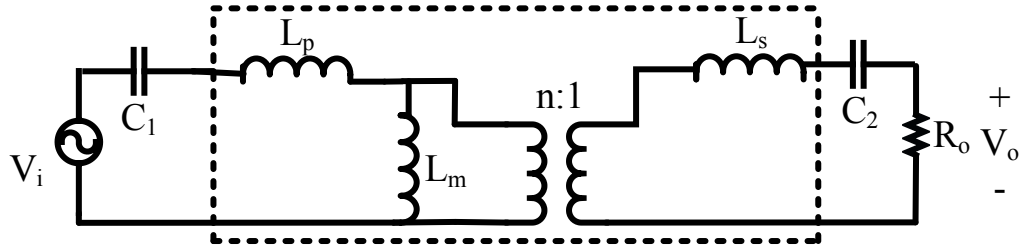
Figure 2-1: Series-series type.

2.2.2   Series-parallel

The idea in this type is to compensate on the primary and make a current path along with compensation in the secondary as shown in Figure 2-2. The advantage of parallel compensation at the load side is to reduce the output voltage ripples while compensating the leakage inductances.
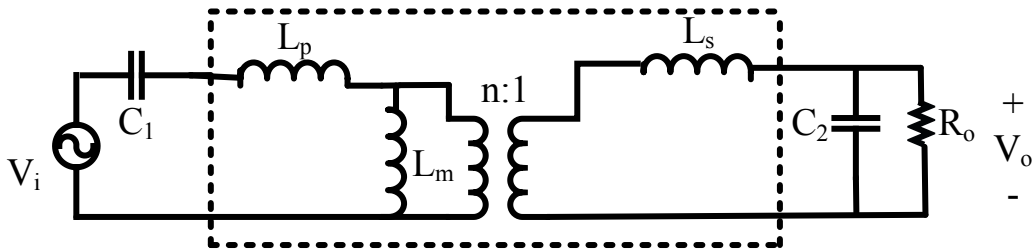
Figure 2-2: Series-parallel type.

2.2.3   Parallel-series type

This type compensates the primary leakage in parallel and the secondary inductor in series. However, as the converters are normally voltage source type, there should be an interface (L_{in}) for the primary side capacitor as shown in Figure 2-3.
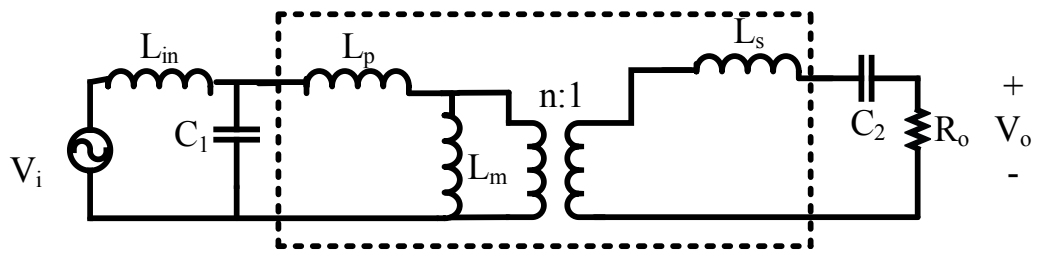
Figure 2-3: Parallel-series compensation.

2.2.4   Parallel-parallel type

Similar to Figure 2-3, in Figure 2-4 the parallel-parallel compensation needs an inductor in series.
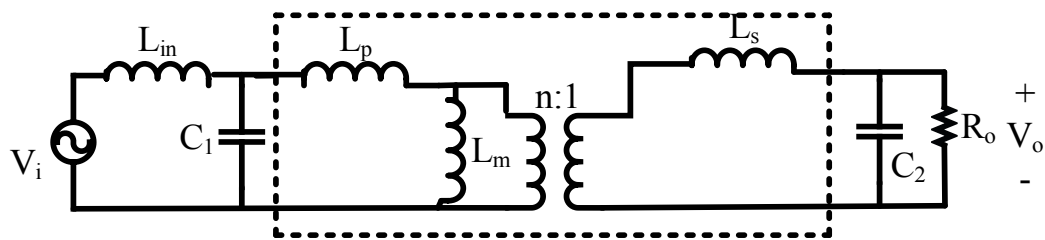
Figure 2-4: Parallel-parallel compensation.

2.3   Series-series compensation types

The circuit in Figure 2-5 shows the model for a two-coil inductive power transfer. It is assumed that the primary and secondary coil resistances (R_p and R_s) are very small.
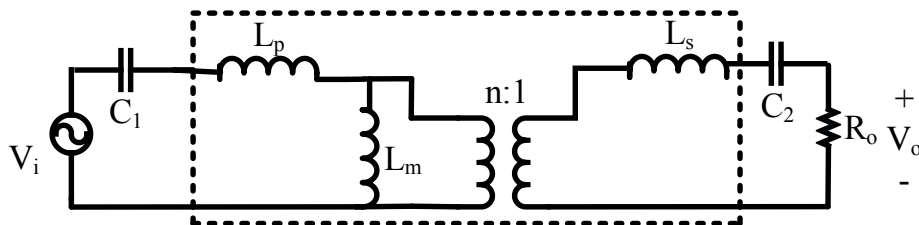
Figure 2-5: First harmonic approximation (FHA) or ac model for IPT

24

To better understand and compare the analysis of this model with the one that will be introduced in chapter 5, it would be good to take a better look at the core of the system, which is the two coupled coils. Two coils can be modeled as mutually coupled inductances as shown in Figure 2-6, or a transformer as in Figure 2-7.
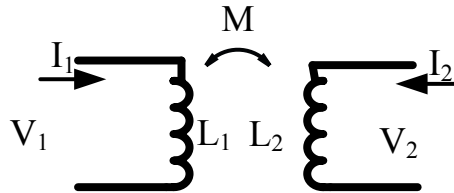
Figure 2-6: Mutual inductance model.
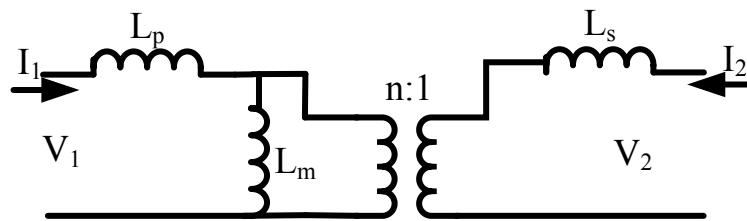
Figure 2-7: Transformer model.

These two models can be related with basic two-port tests using

$$L_1 = L_p + nM$$
Eq. 2-1

$$L_2 = n^2 L_s + nM$$
Eq. 2-2

$$L_m = nM$$
Eq. 2-3

There are two ways to compensate the leakage inductance in this model:

1) To use C_1 to compensate L_p and use C_2 to compensate L_s at the resonant frequency [47], [48]

The objective is to reduce the series elements voltage drop in Figure 2-5 so that the input voltage is reflected to the output only with a turns ratio.

$$C_1 = \frac{1}{\omega^2 L_p}$$

Eq. 2-4

$$C_2 = \frac{1}{\omega^2 L_s}$$

Eq. 2-5
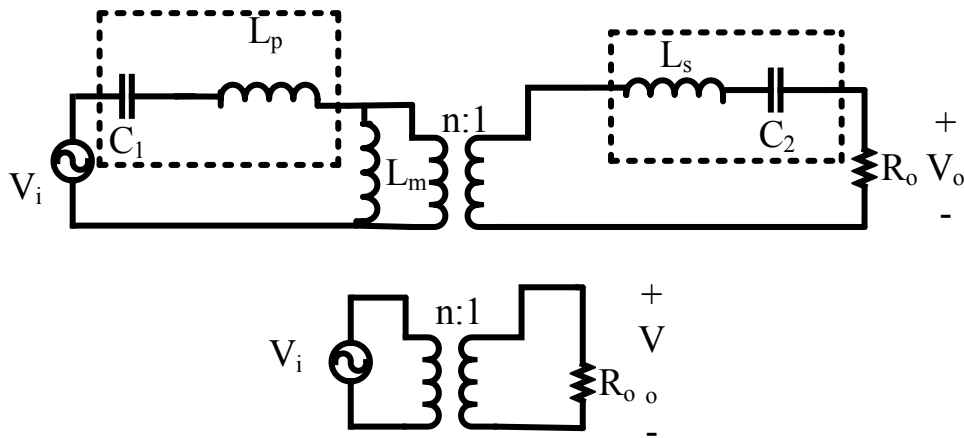
Figure 2-8: Simplified circuit for type 1 compensation.

Although, type 1 compensation (Figure 2-8) is very popular and seems to be reasonable way to get the best efficiency at the output, there is a big disadvantage to it. The output current and output power in this method are highly dependent on R_o. However, the advantage will only be available only if the two simplifying assumptions below are met: a) Assumption that the circuit works exactly at resonant frequency; b) Assumption that there is no leakage resistance; in practice, converter limitations will not let these assumptions become true.

2) Another possibility in series-series compensation is to use C_1 to compensate L_1 and C_2 to compensate L_2 at the chosen resonant frequency [46].

The idea behind this over-compensation (compensation of more than leakage inductance), is to have a current source, independent of the load, rather than a voltage source. By compensating the primary leakage inductance and magnetizing inductance in the primary, a constant current flows at the secondary independent of the load. It is shown in Figure 2-9 that the same amount of impedance is in the primary side's series branch, i.e $-j\omega M$, as the parallel branch. This structure leads to a current source and is called a Boucherot bridge [46].

The compensation that will be used in this chapter, is type 1; because type 1 output voltage sensitivity to frequency change is lower compared to type 2. The frequency response of the different types of compensation is studied in the literature. Series-series compensation tries to transfer the input voltage directly onto the load. The major work that uses parallel compensation is [49], which does not consider switching loss a problem. In this thesis, switching loss reduction will be the main focus for higher frequencies.
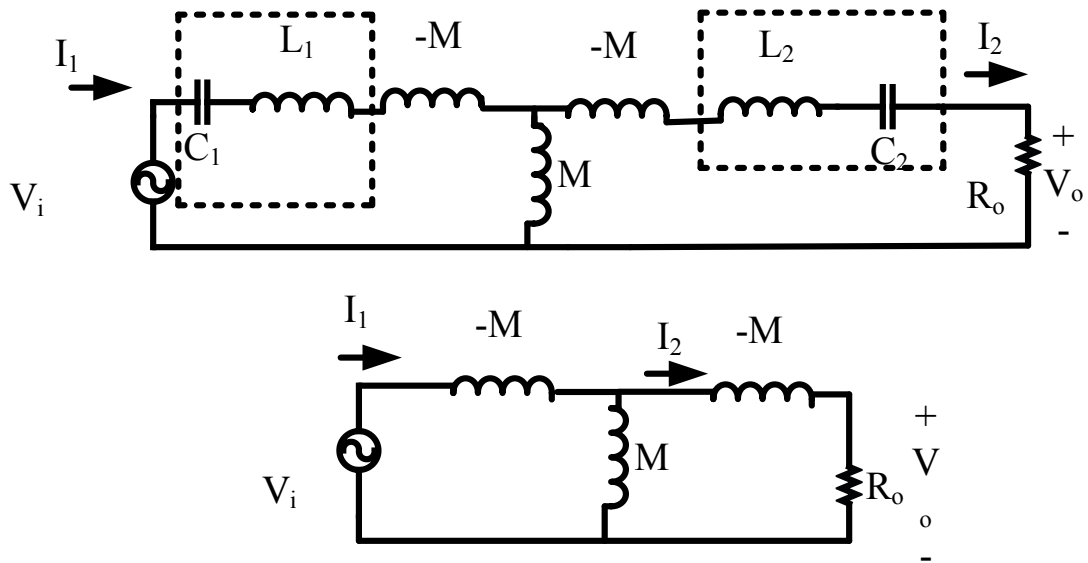
Figure 2-9: Simplified circuit for type 2 compensation.

2.4 Network Analysis

A.1.1   <u>Type 1</u>

The high frequency transformer model is accurate for WPT applications, because in wireless power coils, the distance of the coils is higher than the transformer and thus, the series capacitors that are modeled for high frequency power transformers, have very small impedance in this case and can be ignored. According to [32] and [42], the linear element estimation and FHA are both acceptable assumptions for this study, because the resonant tank will pass only the frequencies very close to designed resonant frequency.

Using first harmonic approximation (FHA), model of the linear elements of the converter, a transfer function can be derived for Figure 2-8. Without considering the turns ratio for simplicity, the transfer function for the output load voltage to the ac input V_i (output of the inverter) can be determined as follows.

$$H_{ac}(s) = \frac{v_o}{v_i} = \frac{s.R_o.L_m}{s.L_m\left(sL_p + \frac{1}{sC_1}\right) + s.L_m\left(sL_s + \frac{1}{sC_2}\right) + \left(sL_p + \frac{1}{sC_1}\right)\left(sL_s + \frac{1}{sC_2}\right)} \qquad \text{Eq. 2-6}$$

$$H_{ac}(s) = \frac{s.R_o.L_m}{s^2\left(L_pL_m + L_sL_m + L_pL_s\right) + s\left(R_oL_m + R_oL_p\right) + \left(\frac{L_m}{C_1} + \frac{L_m}{C_2} + \frac{L_p}{C_2} + \frac{L_s}{C_1}\right) + \frac{1}{s}\left(\frac{R_o}{C_1}\right) + \frac{1}{s^2C_1C_2}} \qquad \text{Eq. 2-7}$$

The transfer function of Eq. 2-7 is a 4th order polynomial, although there are five active elements. As shown in Figure 2-10, three inductors form a cut-set and thus the degree of the circuit is decreased by one.
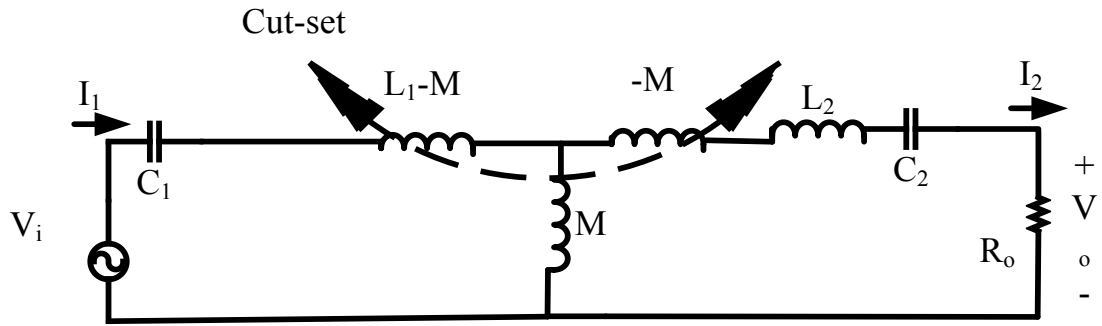
Figure 2-10: Cut-set involving three inductors in type 1 model.

2.5   Zero voltage switching

To decrease the switching loss, the switches are turned on and off at the time when the voltage is zero so that there is minimal power loss at the switch. This method is called zero voltage switching (ZVS). To achieve ZVS for the converter, consider a MOSFET and its internal diode and its parasitic capacitor in Figure 2-11. At the moment of switch turn on, if a negative switch current (I_{switch}) passes through the group of switch, diode and capacitor, this current passes through the diode, which makes the switch voltage V_{DS} equal to negative of the on voltage of the diode before the gate signal rises. So, the switch's voltage and current will never be non-zero at the same time as shown in Figure 2-12.
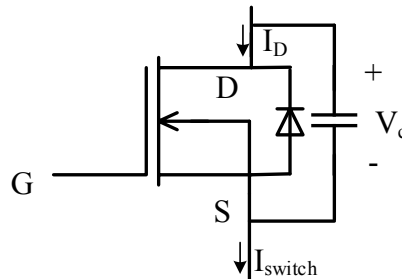
Figure 2-11: MOSFET model

So, when the gate signal is on, the switching loss of the MOSFET and diode are reduced to on-state loss of the diode only.
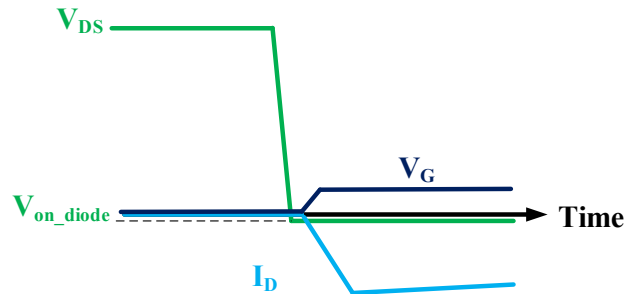
Figure 2-12: ZVS at switch turn on

The capacitor voltage (V_C) is discharged during the on state of the switch. So, when the signal goes from on to off, V_{DS} will show reluctance to rising because of the parasitic capacitor as shown in Figure 2-13. This will reduce the switching loss. The capacitor for the switch can be chosen so that the ZVS at turn-off is realized.

To achieve soft switching, it is necessary that the primary current (I_1) lags the primary voltage (V_i). The phase difference of V_i and I_1 is equal to the phase of the denominator of Eq. 2-7. A typical phase difference graph is shown in Figure 2-14.
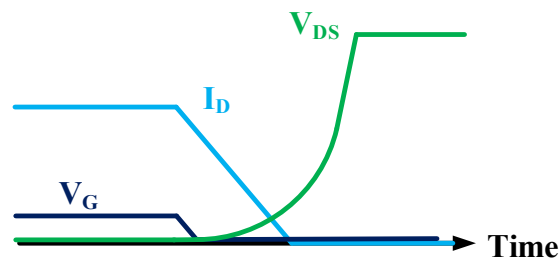
Figure 2-13: ZVS at switch turn off

It can be seen that, in order to achieve soft switching, the operating frequency should be higher than the frequency that the phase is zero. In the specific case that primary

and secondary sides have the same parameters ($L_1=L_2=L$ and $C_1=C_2=C$), by setting the phase of the denominator of Eq. 2-7 to zero, the zero-phase-difference frequency can be derived as Eq. 2-8.

$$f_r = \frac{1}{2\pi\sqrt{LC}}$$

Eq. 2-8
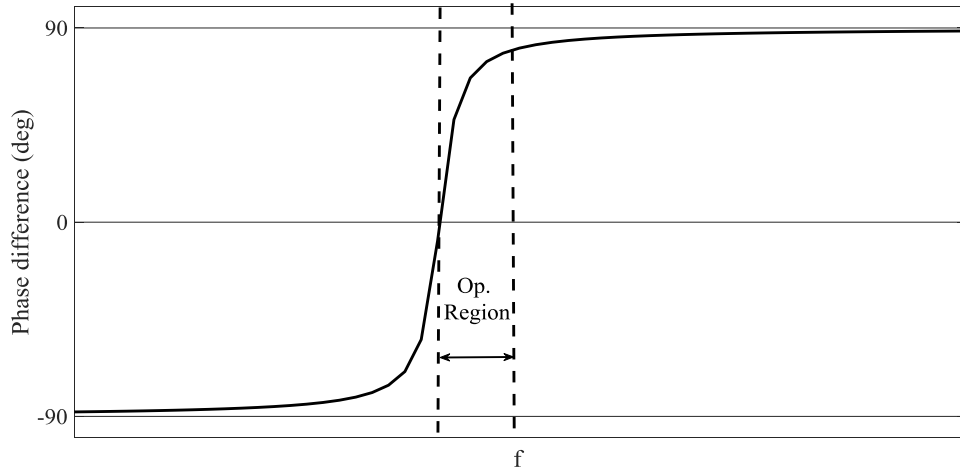
Figure 2-14: Phase difference of V_i and I_1

Thus, the resonant frequency (f_r) is the lower limit for operating frequency, because soft switching is an objective.

Type 2

Using first harmonic approximation (FHA), the resulting transfer function is derived as:

$$|H_{ac}| = \left|\frac{V_o}{V_i}\right| = \frac{1}{\sqrt{\left[Q\left(f_n^4\left(\frac{a_1}{a_2}+n^2(1+a_1)\right)-f_n^2 n^2\left(\frac{a_1}{a_2}+1+2a_1\right)+a_1\right)\right]^2 + \left[f_n^2(a_1+1)-a_1\right]^2}}$$

Eq. 2-9

where:

$$f_r = \frac{1}{2\pi\sqrt{C_1 L_p}} = \frac{1}{2\pi\sqrt{C_2 L_s}} \quad, \quad f_n = \frac{f_s}{f_r}$$

Eq. 2-10

31

$$a_1 = \frac{L_p}{L_m}, \quad a_2 = \frac{L_s}{L_m} \qquad\qquad \text{Eq. 2-11}$$

$$Q = \frac{1}{n^2 R_O} \sqrt{\frac{L_s}{C_2}} \qquad\qquad \text{Eq. 2-12}$$

2.6   IPT Design problem

In IPT systems the distance between the coils and hence the coupling of the transformer are not constant. This can be interpreted by a change in L_m. A possible design approach is to guarantee that for a given range of L_ms, and hence a range of distances between primary and secondary coils, the ac gain of the converter, $|H_{ac}|$ is larger than the minimum requirements at the resonant frequency. This way we can always assure that the output voltage can be controlled at the desired value for all given load conditions. Although in section 2.7, it is shown that the operating point is not necessarily kept at the resonant frequency, the transformer design will be based on the optimal gain at the resonant frequency.

2.7   Control method

After power converter design, control system should be designed to guarantee soft switching and other control objectives such as output power regulation [50]. As we have two degrees of freedom in the amplitude and phase of the current waveform in the tank, we can independently achieve both control objectives. Figure 2-15 shows as schematic of the converter and its control system along with the IPT module. The control loops settle the switching frequency and inverter voltage's (V_{ab}) first harmonic amplitude with the desired power (P_{ref}, Q_{ref}) as the input and primary current (I) as the feedback.
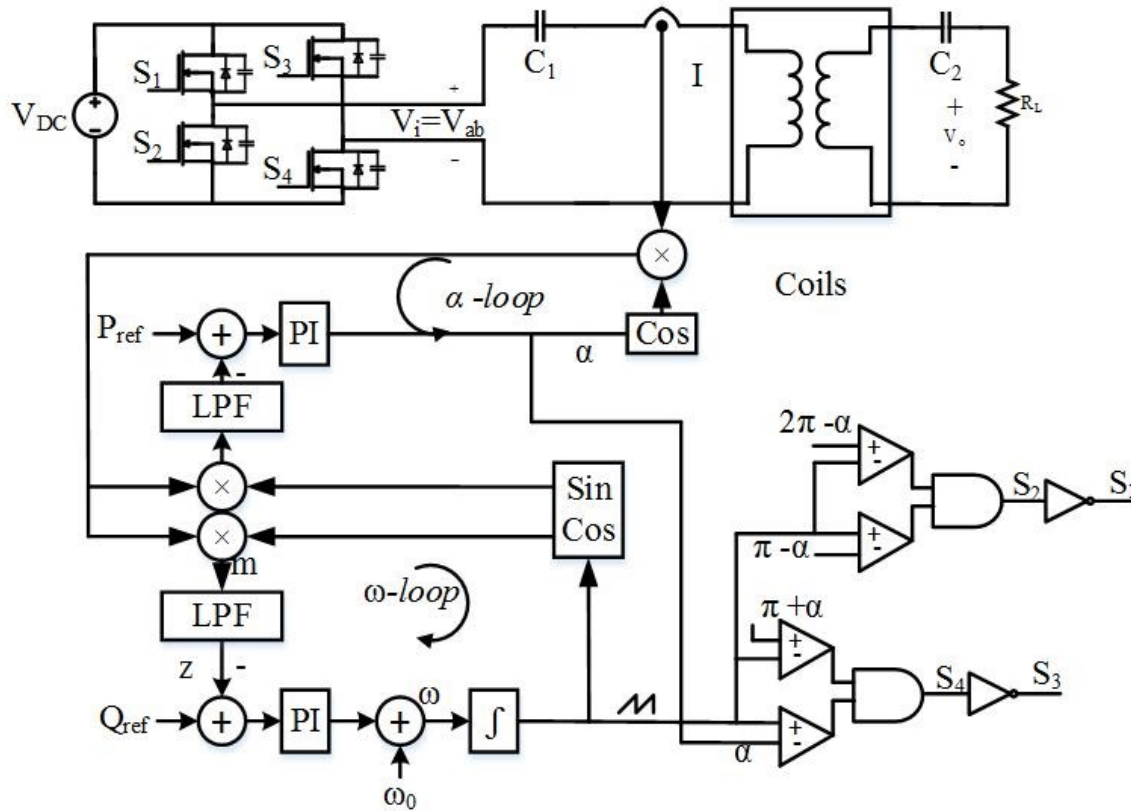
Figure 2-15: Schematic of the whole IPT system.

2.7.1 Proposed control method

In many applications including electric vehicles' application, it is not cost-effective to get the feedback from secondary side. Hence, it is desirable to have only one feedback from the primary side current. Two goals are sought from the current:

a) soft-switching of the inverter

b) set the level of transferred power

The proposed control system logic for forcing the phase difference between voltage and current is shown in Figure 2-16. The fundamental component of the inverter voltage V_{ab} is desired to lead the primary current by γ degrees to guarantee ZVS. The bigger γ is

set, the larger the safety margin for soft switching is. However, if γ is too large, excessive reactive power flows into the circuit, which will in turn reduce the efficiency and will cancel out the benefits of operating above the resonance frequency at ZVS. To set the optimum value for γ, the parasitic capacitance of the switches should be considered [51].To implement the idea in Figure 2-16, the current phase is derived from the feedback signal (I_1) and V_{ab} is shaped through switching with some delay.
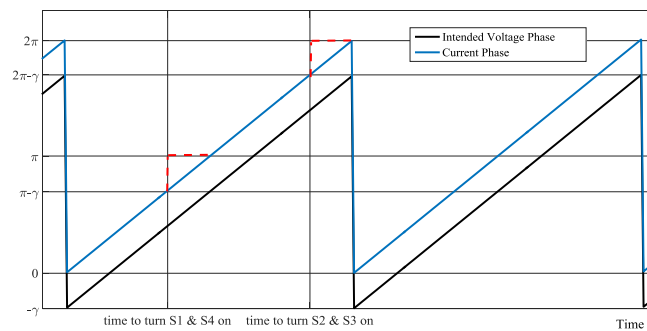
Figure 2-16: The logic of generating inverter signal (switching logic)

The control system in Figure 2-16 controls the converter using:

a) the frequency of the saw-tooth signal (phase control)

b) the firing angle of the voltage α (amplitude control)

The gating logic diagram is shown in Figure 2-17: Complete gating logic without considering voltage amplitude control. It is guaranteed that the DC voltage source is not short circuited, because the switches on one leg are never on simultaneously.

To control the amount of power, the firing angle (α), is used to reduce the amount of voltage's first harmonic. The first harmonic of the voltage is reduced by a factor of $\cos(\alpha)$ if there are two notch levels of $2\alpha/\omega$ seconds as shown in Figure 2-19. In Eq. 2-13, ($2\sqrt{2}/\pi V_{DC}$) is the RMS value of the first harmonic of the full square wave.

$$V_{i,1} = \frac{2\sqrt{2}}{\pi} V_{DC} \cos(\alpha)$$

To achieve this voltage amplitude control, the sawtooth signal generated through ω-loop is compared with α, π-α, π+α and 2π-α to set rising positive edge, falling positive edge, falling negative edge and rising positive edge respectively. Also, the sawtooth signal is altered by γ for soft switching. So, the complete gating logic can be depicted as Figure 2-17.
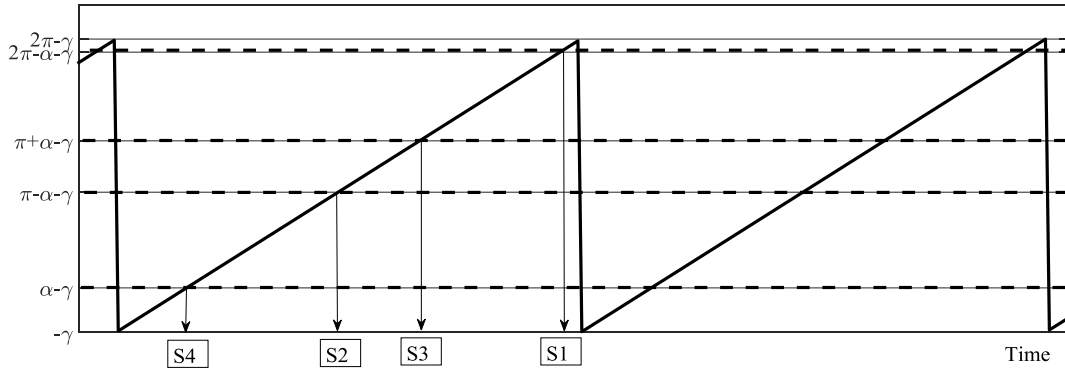
Figure 2-17: Complete gating logic

The gating logic will cause the switches to work in 6 intervals as shown in Figure 2-18. In all intervals, the ZVS is achieved for the switches at turn on and turn off.

The inverter voltage is shown in Figure 2-19. As shown in Figure 2-15, two control loops determine the frequency (f) and the firing angle (α), which are named ω-loop and α-loop respectively. The ω-loop generates γ through an input of Q_{ref} and the α-loop generates α through an input of P_{ref}. The parameter γ is set to make sure there is enough negative current to discharge the parasitic output capacitor to achieve ZVS. Therefore, the value of γ depends on the switch's parasitic capacitor. This determines how much reactive power should be circulated to assure complete ZVS and is controlled by Q_{ref} in Figure 2-15.
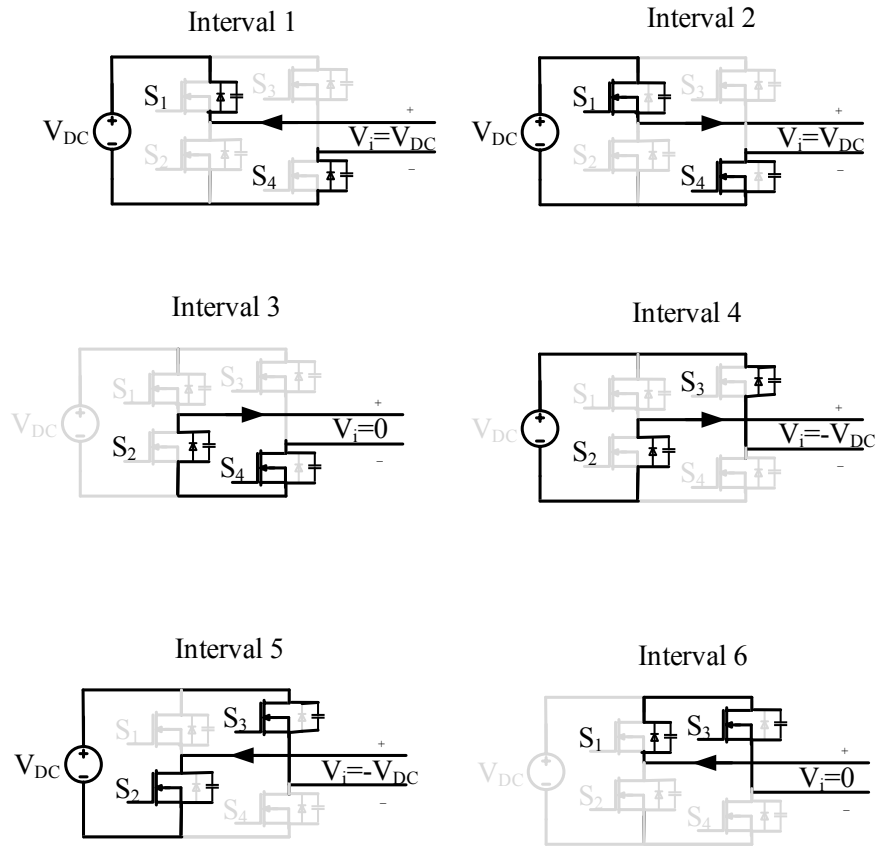
Figure 2-18: Switching intervals
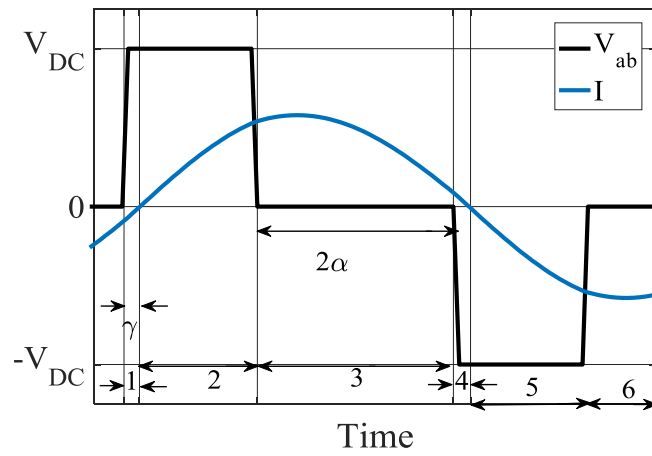
Figure 2-19: Inverter voltage V_{ab} and current.

2.7.2   Control system principle of operation

If the system is stable, it can be proved that both control loops can track a given Q_{ref} and P_{ref} lower than a certain value. Let's assume that the normalized primary current is $\sin(2\pi ft + \phi)$ and the normalized inverter voltage is $\text{sgn}(\sin(2\pi ft + \gamma))$, where γ is the reference phase difference of V_{ab1} and I_1 and ϕ is the actual phase of I_1. As it can be seen in the ω-loop of Figure 2-15, m is a signal that is proportional to the multiplication of normalized current and $\cos(2\pi ft)$:

$$m \sim \frac{1}{2}\left(\sin(4\pi ft + \phi + \gamma) + \sin(\phi)\right)$$ Eq. 2-14

The first term in Eq. 2-14 is at a high frequency and will be filtered out by the low-pass filter. The signal z is derived as:

$$z = \frac{1}{2}\sin\phi$$ Eq. 2-15

Thus the input signal to the PI in ω-loop in Figure 2-15 is $Q_{ref} - \frac{1}{2}\sin\phi$, which will be forced to zero over the time assuming a stable system. This is achieved by changing the frequency. In other words, the integrator changes the frequency $2\pi ft$ so that the actual phase angle between the voltage and current is set to the desired phase value.

The logic in α-loop is similar. The input of the PI is $P_{ref} - P_{actual}$, where P_{actual} is equal to $V_{ab1}I_1$. To reduce the number of sensors V_{ab1} is not measured and its normalized value is estimated by $\sin(2\pi ft)$. If the normalized P_{actual} that is for simplicity shown as P_{actual}, is not equal to the normalized desired power P_{ref}, α is automatically tuned so as to generate a zero error for the normalized transferred power.

2.8   Simulation

A detailed magnetic design process will be discussed in Chapter 4. However to verify the control method only, the design adopted from [46] is approached for fixed values of L_p and L_s and for varying parameter of L_m. It is desired that the gain $|H_{ac}|$ is not lower than 4. Table 2-1 shows the parameters of the resonant tank.
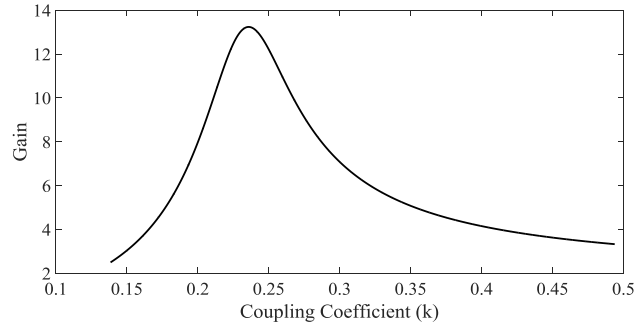
Figure 2-20: Gain variation with coupling coefficient

Gain Variation with only changing coupling coefficient is shown as Figure 2-20. From Figure 2-20, it can be seen that with the desired minimum gain of 4, the range of [0.1653,0.4125] is set for the coupling effect. In other words, the designed transformer should have an L_m in the range of [1.777 μH - 6.388 μH]. The optimum coupling for this design is at k=0.25 or $L_m = 2.88$ μH.

The PI parameters, k_p and k_i of the control design, are 60 and 10^6 for the ω-loop and 3×10^{-4} and 0.8 for the α-loop.

Table 2-1: Circuit elements for .

Parameter	L_p	L_s	L_{r1}	L_{r2}	n	C_1	C_2	f_r
Value	12.57 μH	39.23 μH	4 μH	25 μH	4/10	180 nF	42.6 nF	85 kHz

For P_{ref} set to 200 W and when the transformer coils are located at their optimal distance, where at k=0.25 the gain is maximized, as shown in Figure 2-20.

(a) $L_m = 1.8\ \mu H$ (case 1)   (b) $L_m = 2.8\ \mu H$ (case 2)

(c) case $L_m = 6\ \mu H$ (case 3)
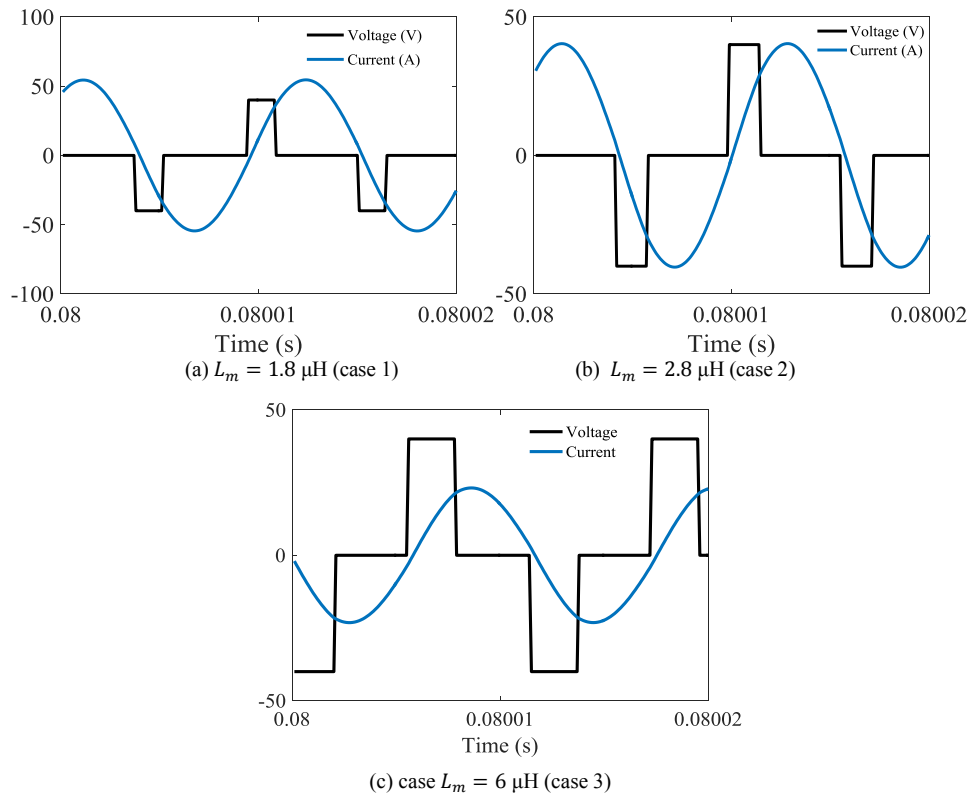
Figure 2-21: Inverter voltage and current in three cases

Comparison of the graphs in Figure 2-21 shows how the control system is maintaining the 10 degrees phase difference so that at the rising edge of inverter voltage, the negative current guarantees soft switching of S_4. Also at the falling edge of inverter voltage, the positive current guarantees soft switching of S_2.

The ZVS is achieved for all cases of Figure 2-21.

For larger L_ms, considering the fact that f_n is larger than unity, the denominator in Eq. 2-9 becomes smaller and hence larger gains are achieved at the output. This can justify the fact that the current in Figure 2-21(b) is smaller than the case of Figure 2-21(a). Same trend can be seen in (c). So, the current simulation results can be justified with the model presented in this chapter.

Also from the viewpoint of the control system, the oscillations in transferred power are damped more easily for the cases of higher coupling. The reason is that the system is stabilized at a narrower voltage signal (higher α). The α-loop generates α equal to 67.8, 63.9 and 54.4 degrees for the three cases respectively.

The power reaches the steady state of 200 W in less than 20 milliseconds. The frequency of all cases is stabilized slightly larger than the nominal 85 kHz, which is 88.00 kHz, 87.57 kHz and 85.26 kHz. This is the cause for observing larger currents at case 2 compared to case 3. The efficiency in case 2 is not better than case 3. The reason is matching loss with the change of L_m although the gain is higher. The efficiency evaluations in Chapter 4 will be meaningful, because the system will be always in matched mode.

Figure 2-22 shows that the system works very well at the power level of 1000 W. Again, the response is settled in less than 20 milliseconds. Even the current level has not increased. Instead, the inverter voltage on width is higher. In other words, α has dropped to 32 degrees.

2.9   Conclusion

In this chapter, a power circuit analysis and control system of a two-coil IPT converter is introduced and discussed based on the physical transformer model. The compensation method is based on series-series capacitors to generate a constant power at the primary in case of ideal resonant frequency operation. Zero voltage switching is explained and its achievement requirement for the proposed topology is derived. The control approach guarantees soft switching and a given reference power to be transferred for all the simulated cases. The method will be easy to implement with only one feedback and for different setups only two PI controllers need to be adjusted.
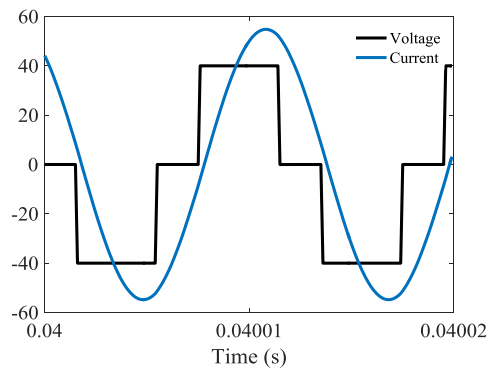
Figure 2-22: Inverter voltage and current in case P=1000 W

CHAPTER 3

IPT MAGNETIC DESIGN

3.1   Introduction

Magnetic design is the core part of the inductive power transfer converter design. The schematic of the studied IPT system is shown in Figure 3-1. The magnetic component in this IPT system is the transformer that needs to be analyzed and designed.
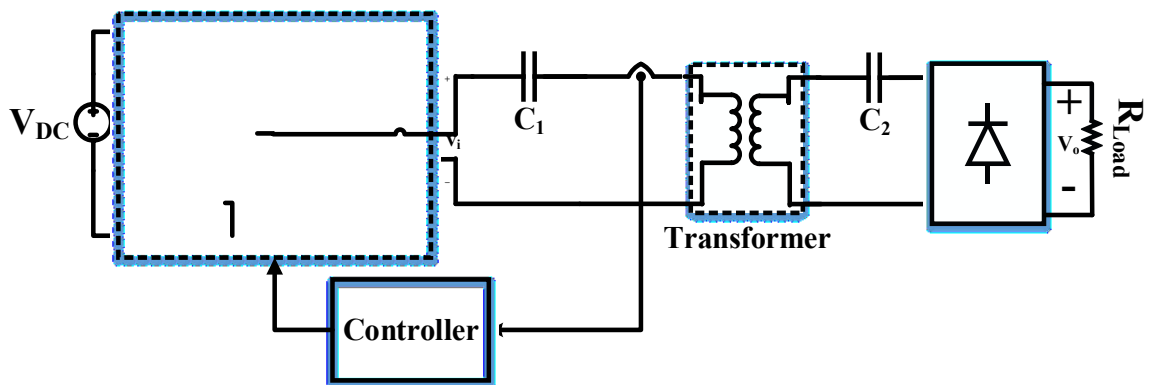
Figure 3-1: Schematic of the designed inductive power transfer.

The algorithm to design a transformer for Figure 3-1 with certain specifications is shown in Figure 3-2. The transformer has to be designed for a specific frequency and power level considering the converter soft switching limitation. To meet these limitation we need to iterate the design process.
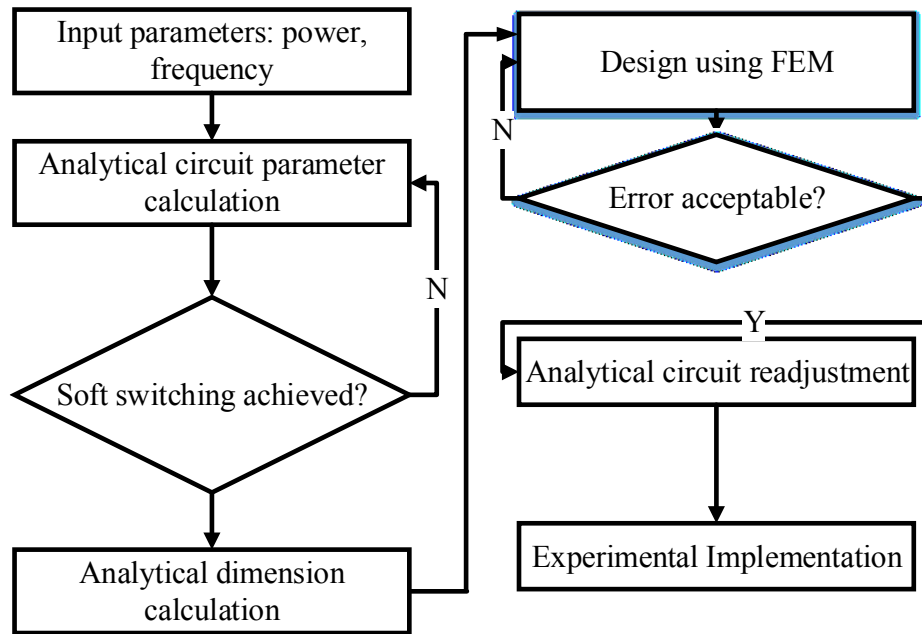
Figure 3-2: Flowchart for magnetic design.

In the following sections, this flowchart is explained in more detail.

3.2 Step by step design for analytical circuit parameter calculation

The objectives of the design will be given as output voltage and output power. The design is supposed to use a constant resistance (R_L) as the load model.

Step 1: The first step is to calculate the nominal load at maximum output power (P_{max}) and nominal output voltage (V_o).

$$R_L = \frac{V_o^2}{P_{max}}$$
<div align="right">Eq. 3-1</div>

In terms of peak voltage, the equation can be rewritten as:

$$R_L = \frac{V_{o,peak}^2}{2P_{max}}$$
<div align="right">Eq. 3-2</div>

Step 2: The second step is to relate the mutual inductance of the transformer to the desired power. Consider the simplified circuit of Figure 3-3.
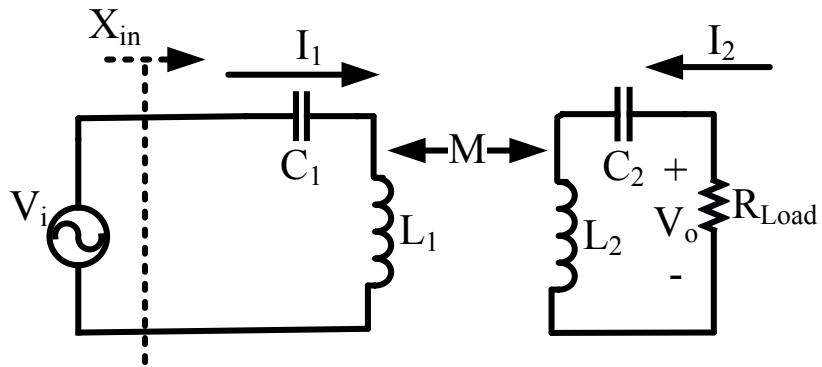
Figure 3-3: AC model of the system for analysis of the transformer.

The method that is used in IPT system is called Boucherot method. The idea is shown in Figure 3-4.
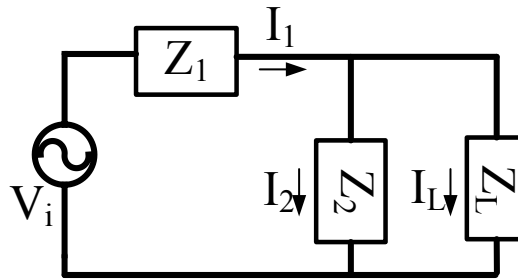
Figure 3-4: Boucherot current source bridge.

In the circuit of Figure 3-4, KVL for the left mesh can be written as:

$$V_i = Z_1(I_L + I_2) + Z_2 I_2 \qquad \text{Eq. 3-3}$$

Assume $Z_1 + Z_2 = 0$ (Boucherot's idea), then the load current can be written as:

$$I_L = \frac{V_i}{Z_1} \qquad \text{Eq. 3-4}$$

Which is independent of Z_L. Comparing Figure 3-4 and Figure 3-3, it is concluded that Boucherot method can be implemented in IPT application by choosing C_1 to compensate L_1.

Mesh analysis of the circuit in Figure 3-3 is shown in Eq. 3-5 to Eq. 3-7.

$$\begin{bmatrix} V_i \\ 0 \end{bmatrix} = \begin{bmatrix} j\omega L_1 + \dfrac{1}{j\omega C_1} & j\omega M \\ j\omega M & R_{Load} + j\omega L_2 + \dfrac{1}{j\omega C_2} \end{bmatrix} \begin{bmatrix} I_1 \\ I_2 \end{bmatrix}$$ Eq. 3-5

$$I_2 = \dfrac{det \begin{vmatrix} j\omega L_1 + \dfrac{1}{j\omega C_1} & V_i \\ j\omega M & 0 \end{vmatrix}}{det \begin{vmatrix} j\omega L_1 + \dfrac{1}{j\omega C_1} & j\omega M \\ j\omega M & R + j\omega L_2 + \dfrac{1}{j\omega C_2} \end{vmatrix}}$$ Eq. 3-6

$$I_2 = \dfrac{-j\omega M.V_i}{(\omega^2 M^2 - L_1 L_2 \omega^2) + j\omega R_{Load} L_1 + (\dfrac{L_2}{C_1} + \dfrac{L_1}{C_2}) + \dfrac{R_{Load}}{j\omega C_1} - \dfrac{1}{\omega^2 C_1 C_2}}$$ Eq. 3-7

In the design process, the operating frequency is assumed to be equal to the resonant frequency, where the load current becomes independent of the load resistance:

$$I_2 = \dfrac{V_i}{j\omega M}$$ Eq. 3-8

From Eq. 3-1 and Eq. 3-8, Eq. 3-9 is derived, whichshows the relation of power to mutual inductance:

$$P_0 = R_{Load} \dfrac{V_i^2}{\omega_0^2 M^2}$$ Eq. 3-9

Where P_0 is the output power at the resonant frequency. Hence, at the end of step two, M can be calculated from other parameters: The output of step 2 is to find M.

$$M = \dfrac{V_i}{\omega_0} \sqrt{\dfrac{R_{Load}}{P_0}}$$ Eq. 3-10

In the third step, the required leakage inductance at the maximum coupling coefficient (k_{max}) should be determined so that the transformer's circuit parameters (L_1, L_2, M) at its worst case (farthest distance) are obtained. The leakage inductance at the primary can be found in terms of L_2 and k_{max} using Eq. 3-11. k_{max} is the maximum coupling coefficient associated with farthest distance and is a given parameter for the design.

$$L_1 = \frac{M^2}{k_{max}^2 L_2}$$
<div align="right">Eq. 3-11</div>

A degree of freedom arises in Eq. 3-11, because there is one equation and two unknowns (L_1, L_2). For experimental considerations, it is compensated with assuming equal leakage inductances for the coil, meaning that the coil parameters matrix is symmetrical, i.e. $L_1 = L_2$.

It is shown in Figure 3-5 that the idea of having equal leakage inductances is good from the viewpoint of input impedance. The frequency response of the input impedance (X_{in}) in smallest in case of equal leakage inductance. The assumption made in this graph is fixed k (coupling coefficient).
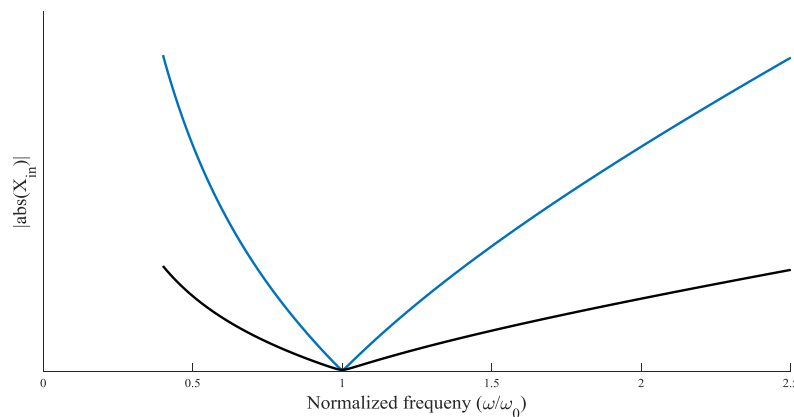
Figure 3-5: Frequency response for the case $L_1 = L_2$ (black), for the case $L_1 = 10L_2$ (blue).

The fourth and last step of the design is to design the capacitors. For full compensation of leakage inductances, C_1 and C_2 are obtained through:

$$C_1 = C_2 = \frac{1}{L_1 \, \omega_0^2} \qquad\qquad \text{Eq. 3-12}$$

The novelty of this design process lies in its capability to calculate inductor and capacitor directly from power and voltage inputs. This design is customized for series-series compensation for IPT and does not apply to other topologies. Also it should be noted that the coils from this design are similar, which makes building the experimental prototype easier.

3.3   Soft switching condition for the converter

As discussed in Chapter 2, the converter produces an ac voltage whose frequency and firing angle can be controlled (V_i in Figure 3-3). The design parameters obtained in section 3.2 should guarantee soft switching within a certain range for frequency, feasible voltage range for the capacitors, and feasible current range for the converter. The bottom-line for this part of design is the price, i.e. if the designed parameters do not satisfy the objective power (assuming that the control method pushes the frequency to a level that soft switching is achieved) in the simulations, it is need to go back to the design section and increase P_{max}.

As mentioned in the algorithm, if the circuit elements from 3.2 are not satisfying the soft switching condition, one should reconsider the design parameters for the converter. This can be realized by varying L_1 and L_2. If the one degree of freedom is used so that the two leakage inductances are not equal, mathematically infinite alternative solutions exist. This makes the design process iterative, and the designer can change the pair of L_1 and L_2

many times so that a cheaper design is achieved. Other than the price, the voltage stress on the capacitors must be taken into consideration, because those are among the other design limits.

To make sure that all design objectives are satisfied we accurately simulate the converter with the transformer. The following criteria are checked in simulation to verify the design:

- Frequency of the converter does not exceed 1.2 times the resonant frequency

- Voltage of the capacitors do not exceed 5 times the input DC voltage

- Power control tracking is achieved with zero error.

3.4   Analytical dimension calculation

Approximations of Neumann integral can be found in [52], [53] and [54]. One of the simplest rules for analytical methods is the Greenhouse method [53], where the net mutual inductance is set to the sum of mutual inductance of any two parallel conductors. Customized variations of Neumann formula for shapes like rectangular spirals can be found in [38], [55] and [54]. For the specific shape used in this thesis (flat rectangle with circular cross-section wires), the self-inductance is calculated using an approximate method introduced in [51].

$$L=\frac{N^2 \times 2 \mu_0 D_{avg}}{\pi} \left(\text{arcsinh} \left(\frac{D_{avg}}{2R} \right) \text{-1} \right)$$ Eq. 3-13

Where D_{avg} is the average of inside length (D_i) and outside length (D) as shown in Figure 1-12, and R is the equivalent radius of the litz wire, and N is the number of turns. It is assumed that the winding of the coil is tight (no spacing between the wires). Therefore,

two identical windings with the same self-inductance are to be built. There is two degrees of freedom, as D_{avg} R and N are design parameters, and there is only one equation.

3.5   Design using FEM

The design obtained in section 3.4 should be verified with finite element method (FEM). FEM enables solving numerical problems including partial differential equations using mesh analysis.

3.5.1   Ampere's Law, self- and mutual inductance

For finding the self- and mutual inductance of coils, the Ampere's law is applied to a volume. Ampere's law in partial differential form is shown as in Eq. 3-14 [56].

$$\nabla \times B = \mu_0 J$$ Eq. 3-14

In Eq. 3-14, $\nabla \times$ is the curl sign, μ_0 is vacuum permeability and J is the current density vector assigned to each point. With all the current density in a given volume known and through Eq. 3-14, magnetic flux density vector (B) at each point can be derived. However, partial differential equations are very complicated. So, magnetic design software is used to solve these equations. The post-process of this solution would be to calculate the self- and mutual inductance. The equations for this post-process is given in Eq. 3-15 and Eq. 3-16 [57].

$$L = \frac{\Psi_1}{I_1}$$ Eq. 3-15

$$L = \frac{\Psi_2}{I_1}$$ Eq. 3-16

In Eq. 3-15 and Eq. 3-16, Ψ_1 and Ψ_2 are called self flux linkage and mutual flux linkage respectively. These magnetic flux linkages can be derived for a simple structure of

Figure 3-6 as in equations Eq. 3-17 and Eq. 3-18. dS is the normalized vector perpendicular to the surface of each coil.
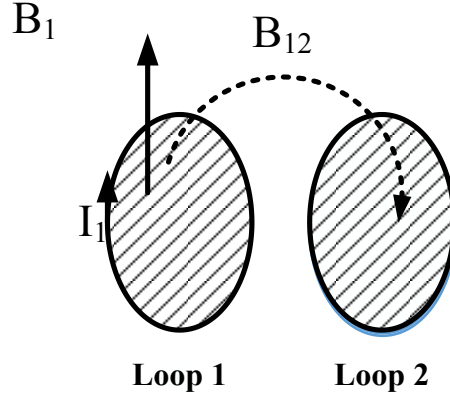
Figure 3-6: Flux density vectors caused by a current in two coils.

$$\Psi_1 = \int_{Loop1} B_1 . dS \qquad\qquad\text{Eq. 3-17}$$

$$\Psi_2 = \int_{Loop2} B_{12} . dS \qquad\qquad\text{Eq. 3-18}$$

It should be noted that Eq. 3-17 and Eq. 3-18, all the existing flux density comes from loop 1 current I_1.

Both the numerical differential equation solution (Eq. 3-14) and the post process (Eq. 3-15 to Eq. 3-18) calculations are developed by the software ANSYS Maxwell.

3.5.2   Finite Element Method

Finite element method is applicable to boundary value partial differential problems. Rewriting Eq. 3-14 in Cartesian coordinate system, the three equations Eq. 3-19, Eq. 3-20 and Eq. 3-21 are obtained.

$$\frac{\partial B_z}{\partial y} - \frac{\partial B_y}{\partial z} = \mu_0 J_x + \frac{\partial E_x}{\partial t} \qquad\qquad\text{Eq. 3-19}$$

$$\frac{\partial B_x}{\partial z} - \frac{\partial B_z}{\partial x} = \mu_0 J_y + \frac{\partial E_y}{\partial t}$$ Eq. 3-20

$$\frac{\partial B_x}{\partial y} - \frac{\partial B_y}{\partial x} = \mu_0 J_z + \frac{\partial E_z}{\partial t}$$ Eq. 3-21

Where B_x, B_y and B_z are the components of flux density; E_x, E_y and E_z are components of electric field; J_x, J_y and J_z are components of electric current density; It should be noted that Eq. 3-19, Eq. 3-20 and Eq. 3-21 are true for every point in the space. In this study, the time derivatives of electric field can be ignored, because the static inductances of the coils are to be derived.

The geometry of the problem is given to a numerical software (ANSYS Maxwell), to solve the equations Eq. 3-19 to Eq. 3-21. Through this, the self- and mutual inductance of the designed coils can be verified.

3.6   Case study design problem

It is desired to design a 100 W IPT system with parameters of Table 3-1.

Table 3-1: System prarameters.

Output power	0-100 W
Input voltage	25 V DC
Output voltage	20 V AC
Maximum matching factor	0.2

Following the instructions and assuming equal inductances for simplicity, the first iteration gives circuit elements like in Table 3-2.

The step by step design process is shown in the next page.

51

$$R_L = \frac{20^2}{100} = 4 \ \Omega \qquad \qquad \text{Eq. 3-22}$$

$$M = \frac{25}{2 \pi 70000} \sqrt{\frac{4}{100}} = 11.368 \ \mu H \qquad \qquad \text{Eq. 3-23}$$

$$L_2 = L_1 = \frac{M}{k_{max}} = \frac{11.368}{0.2} = 56.84 \ \mu H \qquad \qquad \text{Eq. 3-24}$$

$$V_i = \frac{2\sqrt{2}}{\pi} V_{DC} = 22.5 \ V \qquad \qquad \text{Eq. 3-25}$$

$$C_1 = C_2 = \frac{1}{4 \pi^2 f^2 L_1} = 90.94 \ nF \qquad \qquad \text{Eq. 3-26}$$

Table 3-2:circuit elements

L_1	L_2	C_1	C_2
56.84 µH	56.84 µH	90.94 nF	90.94 nF

To make sure that the transformer and capacitor designs work, first an open-loop simulation is done in PSIM to get the maximum output power. The schematic is the same as Figure 3-3 and it is assumed that a clear sinusoidal waveform is the input of the circuit.

Important circuit variables for voltage stress are V_{C_1} and V_{C_2} which are shown in Figure 3-7 and Figure 3-8.

Providing 91 nF capacitor with a rating above 200 V is feasible, so we can proceed with the design parameters.

It can be seen that the first harmonic approximation was a good method, because the coils act like a filter and let the resonant frequency to pass only, which is the reason for sinusoidal waveforms of Figure 3-7 and Figure 3-8.
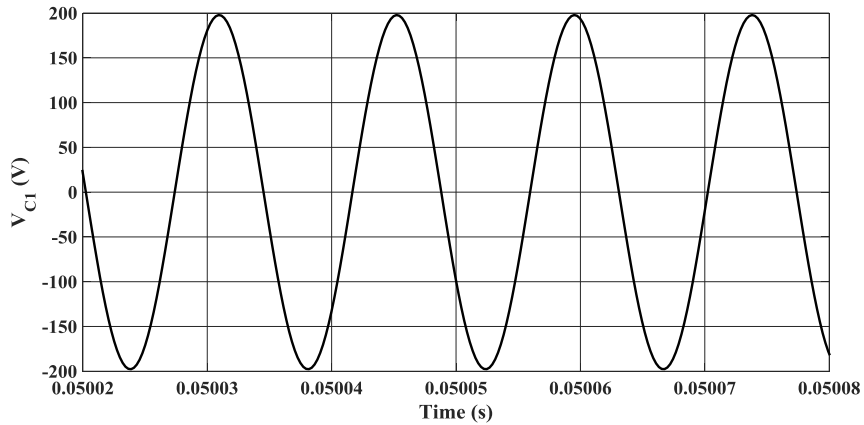
Figure 3-7: Primary capacitor voltage.
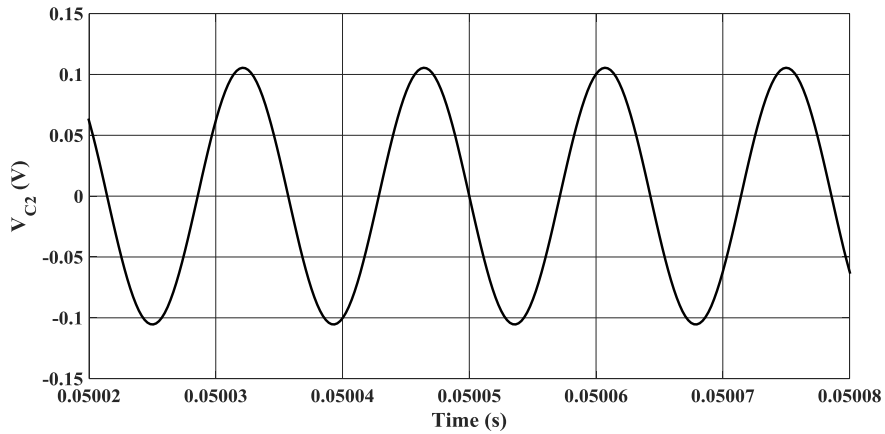
Figure 3-8: Secondary capacitor voltage.

Also the open-loop load current is shown in Figure 3-9.

The coils shown in Figure 3-10 show the magnetic design with ANSYS Maxwell that provide the electrical circuit elements very close to what is desired in Table 3-2. The coil turns and dimensions and the resulting parameters from the software are shown in Table 3-3.
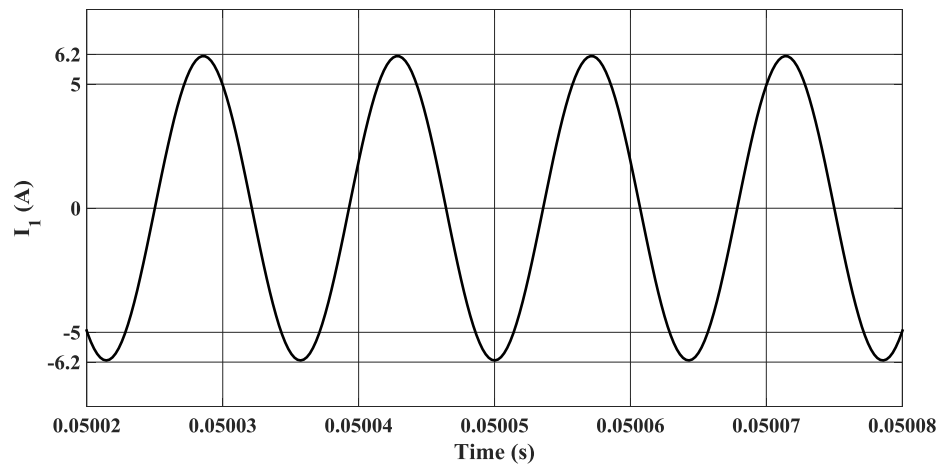
Figure 3-9: Primary current

Ansys Maxwell simulation was based on flat square coil and was done along with building the experimental setup. The medium around the coils were set a one meter cube so that the flux density boundary condition does not affect the validity of the results.
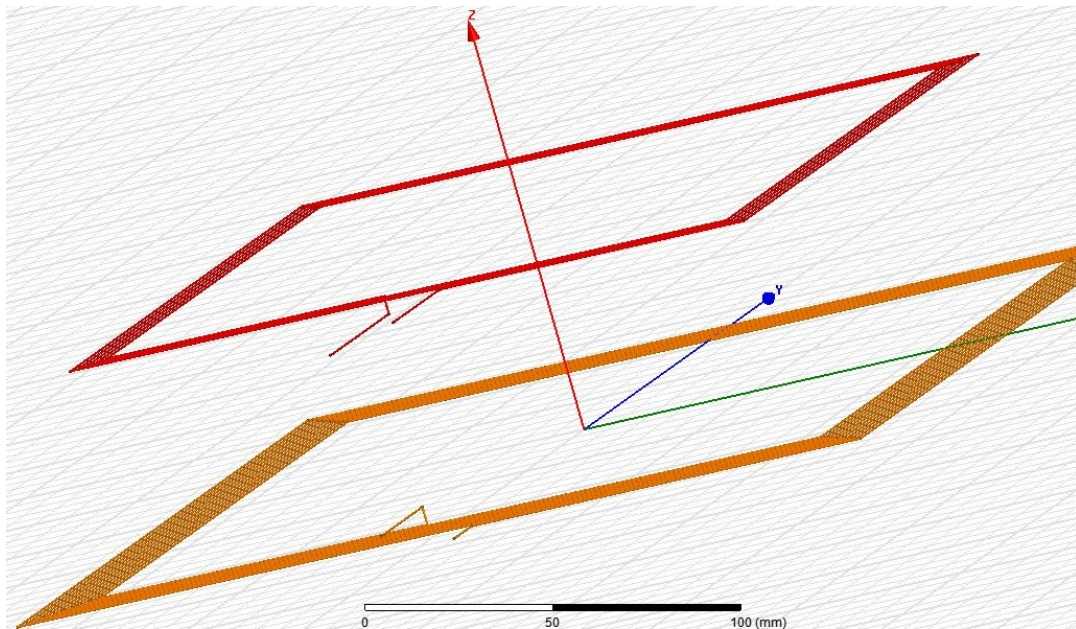
Figure 3-10: Schematic of the magnetic design

Table 3-3:Simulated coil in Maxwell

Number of turns in each coil	10
Exterior coil length	250 mm
Interior coil length	210 mm
Distance between two coils	32 mm
L11	61.91 µH
L12	13.79 µH
L21	13.79 µH
L22	61.91 µH

The schematic of the closed-loop test circuit is shown in Figure 3-11.
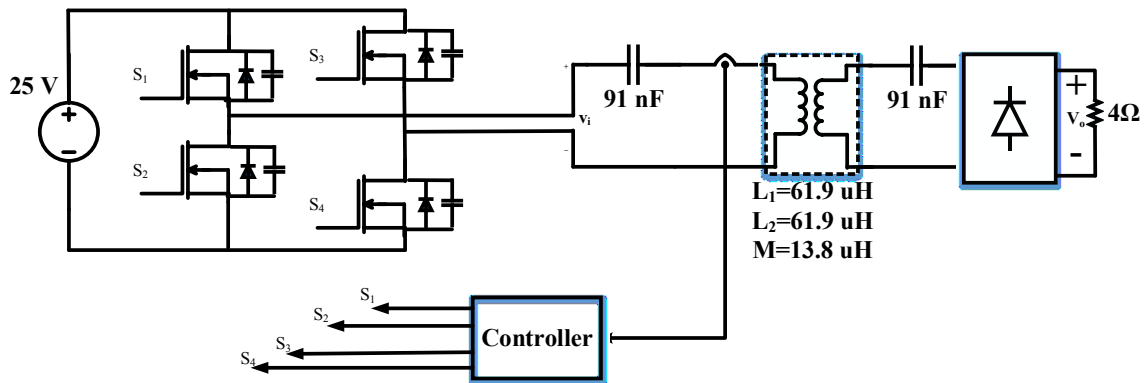
Figure 3-11: Circuit model for the whole system

The parameters for the controller in this case are also shown in Table 3-4. k_{IQ} and k_{IP} are the integrator coefficients of the α-loop and ω-loop PI respectively. k_{IP} and k_{PP} are the proportional coefficients of the α-loop and ω-loop PI respectively. The filters' cut-off frequencies are set so that they include the switching frequency.

Table 3-4: Closed-loop parameters.

k_{IQ}	1.5e6
k_{PQ}	1.52e2
ω-loop filter Cut-off frequency	140 Hz
k_{IP}	1.75
k_{PP}	5e-3
α-loop filter Cut-off frequency	140 Hz
P_{ref}	45 W

The reference power and soft switching are both satisfied in this case, which is shown in Figure 3-12.
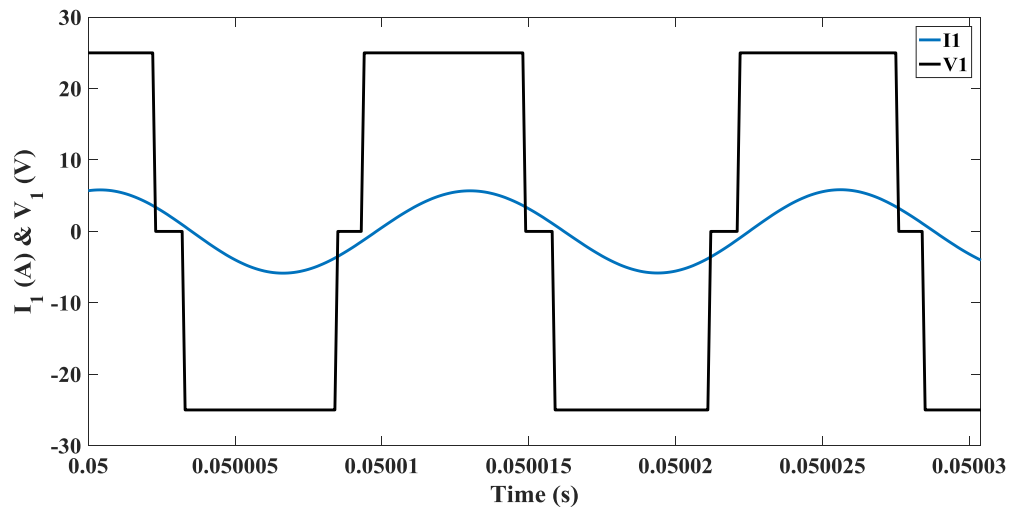
Figure 3-12: Primary current and voltage

The primary current in Figure 3-13 is a bit off-sinusoidal, because the resonant tank (the coils) are not ideal and have passed little portions of the input signal harmonics.
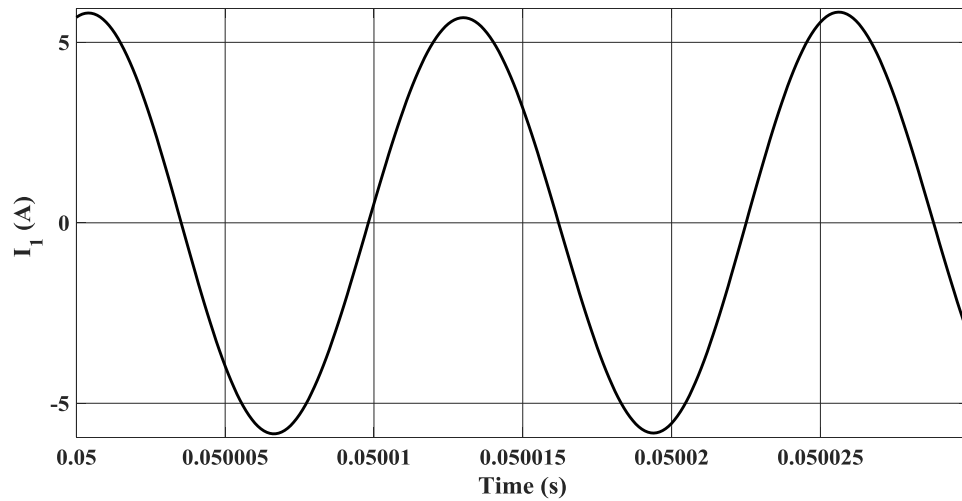
Figure 3-13: Primary current

The off-sinusoidal shape of the current is due to the fact that it is working off-resonance frequency (79.1 kHz). Load current graph is shown in Figure 3-14.
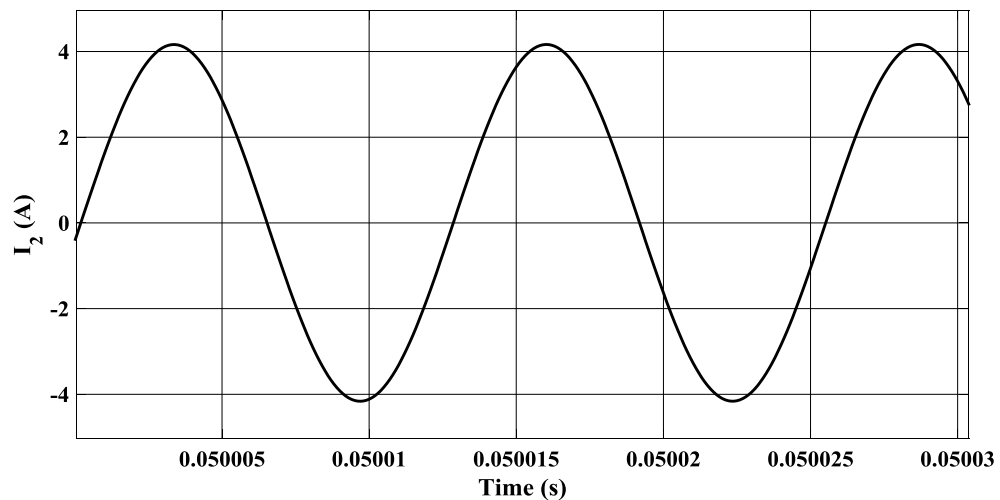
Figure 3-14: Secondary current.

System frequency settles at 77.9 kHz in less than 10 milliseconds. In addition, it can be seen that the secondary current is 84 degrees lagging the primary current which is close to theory in which the phase difference is 90 degrees at resonant frequency.

3.7   Experimental Results

The same case study is experimented through the setup shown in Figure 3-15. The coil visible at the top is the load coil and an almost identical source coil is sitting on the table with a distance of 30 millimeters. The step by step design was done for the case of resonant frequency of 70 kHz and power of 0 to 100 Watts. The resulting load is a 4 ohm rheostat on the right side of the table and the capacitors are selected 91 nF; the secondary is attached to the rheostat and the primary is connected to the inverter. The RLC meter shows that the primary side inductance L_1 is 70.54 µH and the secondary is 73.20 µH and both coils have 0.8 ohm resistance. The measured values for the leakage inductances and capacitors are and tabulated in Figure 3-6.
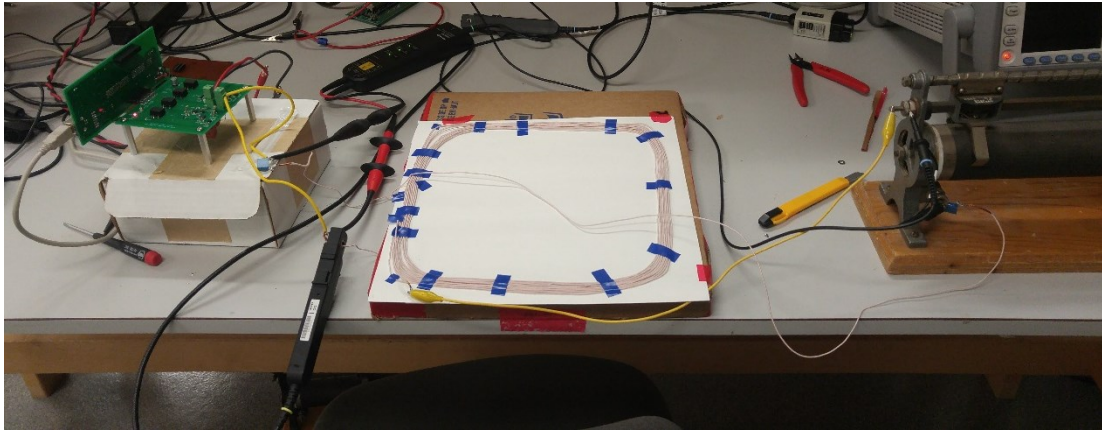
Figure 3-15: Experiment setup.

Table 3-5: Measured circuit parameters.						
L_1 (µH)	R_1 (Ω)	L_2 (µH)	R_2 (Ω)	C_1 (nF)	C_2 (nF)	R_{Load} (Ω)
70.54	0.78	73.20	0.81	92.57	93.18	3.99

Sensing the feedback current was the biggest issue in the experiment. The high sampling frequency like the one used in PSIM simulations (1 MHz) caused the processor not be able to do all the simulations in practice. To address this problem, only the ω-loop related part of the control system was processed with 1MHz frequency, and the rest was processed with 400 kHz. The ω-loop calculations need to be done in every 70 kHz period (at least 2 samples with the Nyquist rate, which is best case).while the α-loop does not need to be that fast, because power tracking error can be tolerated for thousands of cycles. The processor (TI 28335) could handle operations with 150 MHz bandwidth, so, the number of operations with both control loops is critically close to the bandwidth of the processor. With slowing one loop down, the operations are doable for the processor.

The case of 45 W is experimented and the voltage and currents in primary is shown in Figure 3-16 and load variables are shown in Figure 3-17. The switching frequency is 77.1 kHz.
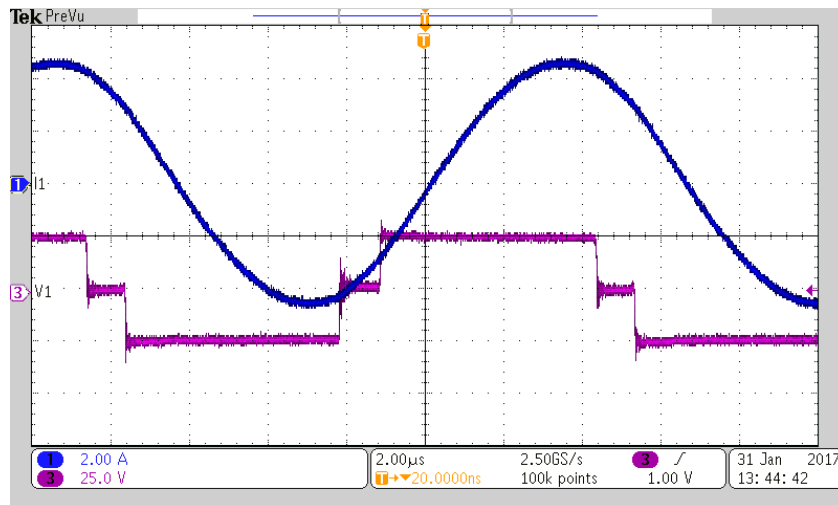
Figure 3-16: Primary voltage and current for case 45 W
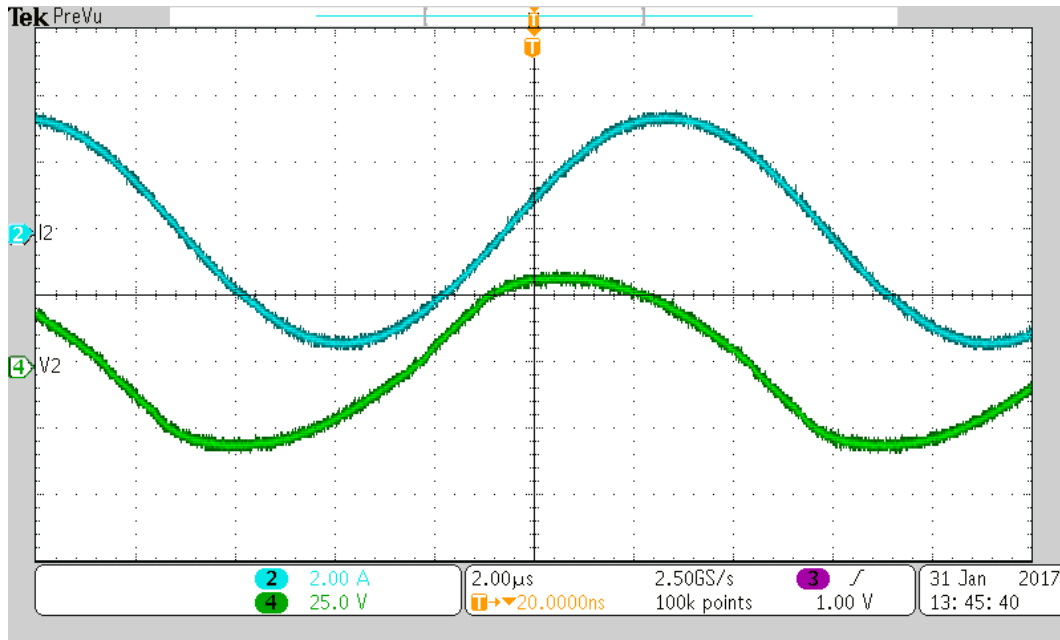
Figure 3-17: Load voltage and current for case 45W

One interesting phenomenon observed in load current and voltage, is the phase difference, which is due to the highly inductive effect of the load (1.18 µH) in high frequency.

The settled frequency is 73.8. The efficiency of the IPT system according to the oscilloscope is 71% which is acceptable with the excessive leakage inductance in all the connecting wires. The input power is 42.51 and the output power is 35.24 W.

The primary side waveforms for the case of 52 W input power is shown in Figure 3-18. The frequency at this case was set to 74.8 kHz. The input power is measured at 51.68 W and this is almost the maximum power that this IPT setup can handle. The reason is the design is being compromised for ZVS, and cannot reach its nominal input power, because it should not work at resonant frequency. ZVS is achieved by the controller, because all switches turn on when a negative current is sunk from the switch's diode.
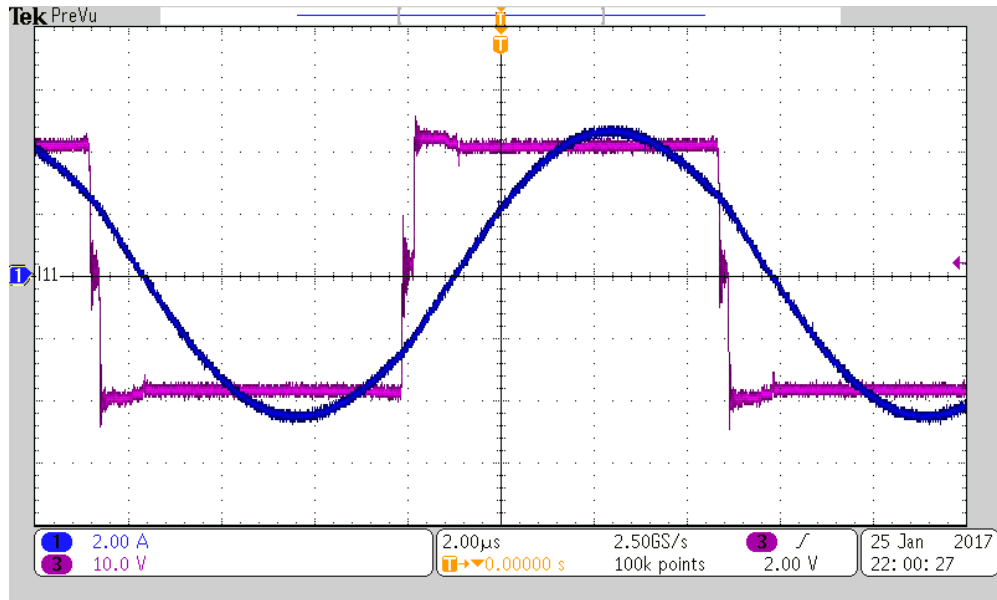
Figure 3-18: Primary side waveforms for case: 52 W

The output voltage for this case is shown in Figure 3-19. The output power of 42.5 W and efficiency of 82% is achieved at this case.
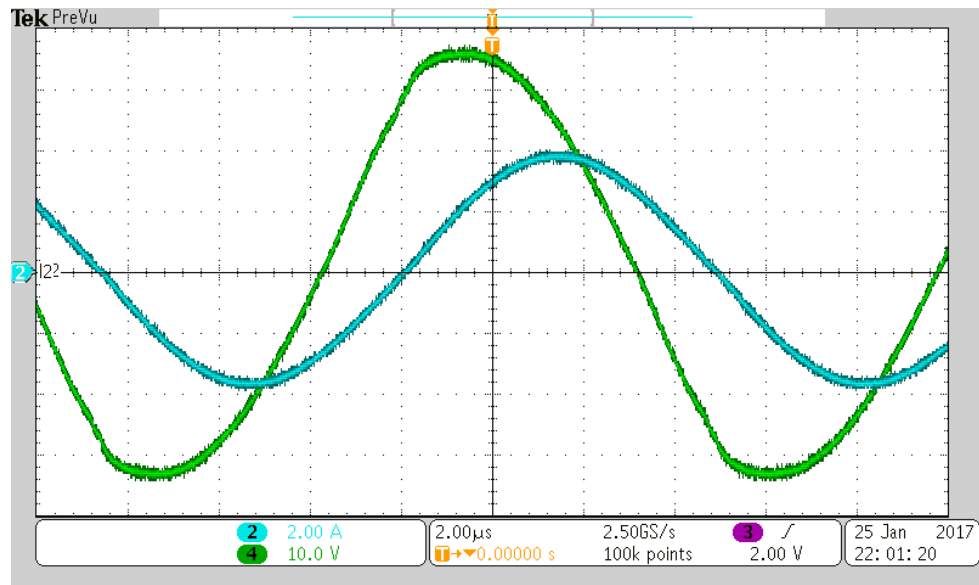
Figure 3-19: Load side waveforms for case: 52 W

The last case's waveforms are shown in Figure 3-20 and Figure 3-21 for an input power of 16.40 W.
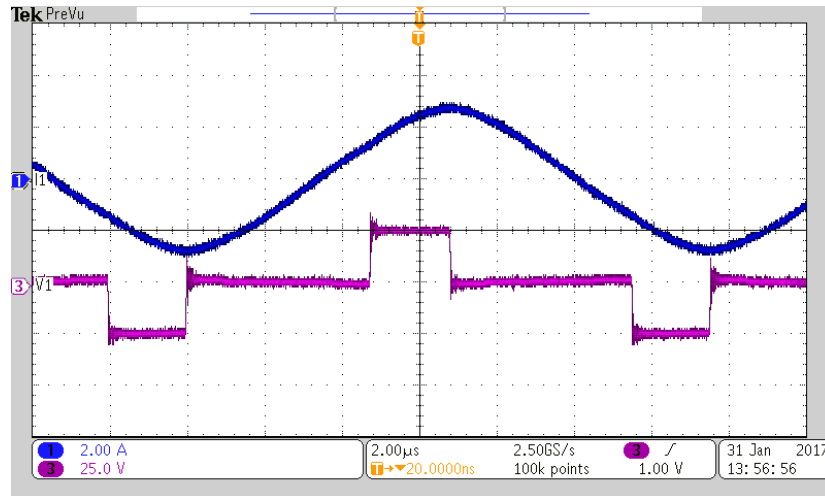
Figure 3-20: Load side waveforms for case: 52 W

The frequency is 73.8 kHz and output power and efficiency are at 14.28 W and 87.07% respectively.
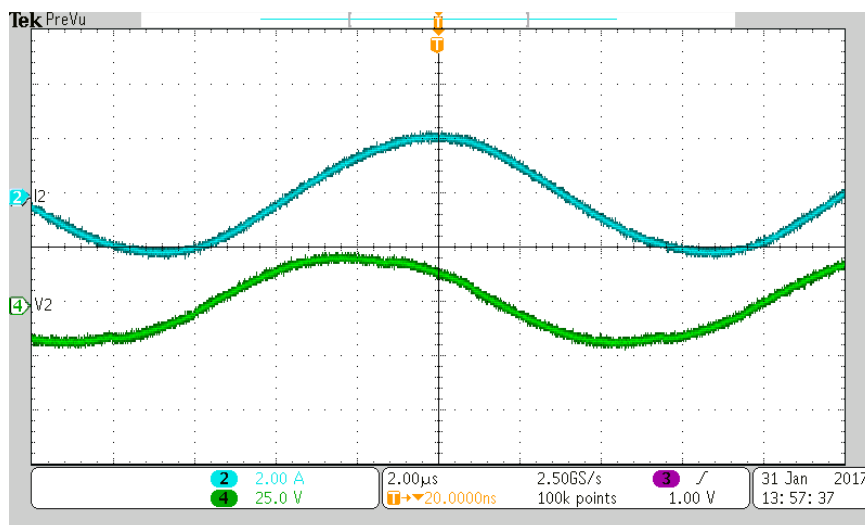
Figure 3-21: Load side waveforms for case: 52 W

The common phenomenon among the three cases of the experimental results are achievement in ZVS. Comparison of the three cases show that efficiency is higher when the controller sets the frequency closer to the resonant frequency.

3.8   Conclusion

In this chapter, a simple step by step approach for designing the magnetic part of the IPT and converter setup is explained. The method can work with given values of inductances and is highly sensitive to the input values. A magnetic design process was introduced, based on which a 20 V-100 W setup was implemented. The magnetic design simulations using Ansys Maxwell were verified in practice. The converter simulations were done with PSIM and the whole system was implemented on a TI 28335 processor. The results were slightly different from simulation because of parasitic circuit parameters involved and also the non-ideal current sensors. However, the control system was settled and ZVS was achieved in all cases. The closer the controller settles the frequency to resonant frequency, the higher the efficiency of the setup will be.

CHAPTER 4

RWPT APPROACH

4.1   Introduction

As discussed in chapter 1, resonant wireless power transfer (RWPT) systems have attracted significant attention in recent years for applications such as home appliances and hybrid vehicles battery charging [58]. There are many papers in the literature which analyze the efficiency and performance of RWPT systems with circuit models analysis. Normally the circuit model is presented and analytical results are compared with the experimental system in terms of loss and efficiency [59]. In another approach, the circuit model is presented and the efficiency of the indirect-fed WPT is studied under different distances and operating frequencies, and for two different WPT systems with very high resonant frequencies in the range of megahertz [19]. In most of the existing approaches the circuit is studied in great detail. However, they do not explain the relationship of the dimensions and positions of the structure with the circuit parameters. Hence, while useful RWPT analysis tools are presented in [19] and [59], no design instruction is presented. Although applied to very high frequency, a direct dimension-related analysis is demonstrated in [60] for the mutual inductance and the performance of a wireless power transfer system with two impedance matching units. Neumann formula is the basis of [60] and the objective is to achieve the maximum efficiency.

Few papers have presented the design process for RWPT. A design approach for RWPT in a transit bus charging system has been introduced and implemented in [13] with details on the management issues of where and how to charge the batteries of the buses. However, unlike the research in [59]-[60], the design in [61] is done for a WPT with a core which delivers power more efficiently. In this chapter, the design problem for a coreless indirect-fed RWPT is studied with the goal of minimizing the coil size. Unlike most papers in the literature, the delivered power is chosen as one of the design inputs rather than efficiency. The reason is that in practice, loads need a minimum power. Therefore, in this chapter, the circuit model analysis along Neumann formula are used to design a RWPT capable of delivering a minimum Pout to the load in an optimally-sized system. The characteristics of the WPT system with respect to changes in coil size is explained analytically. A design approach is also introduced to determine the optimal size without time-consuming design process.

4.2   An indirect-fed resonant wireless power transfer design problem

Designing a wireless power transfer unit includes many details. The unit to be designed, is a resonant wireless power transfer (RWPT) system with four resonant circuits (indirect-fed type). The WPT unit contains four coils:

1) A source loop which is electrically connected to the AC source;

2) A sending resonant coil;

3) A receiving resonant coil; and

4) A load loop which is electrically connected to the load.

These loops will be referred to with their corresponding numbers in this chapter. Figure 4-1 shows the schematic view of the system to be designed.
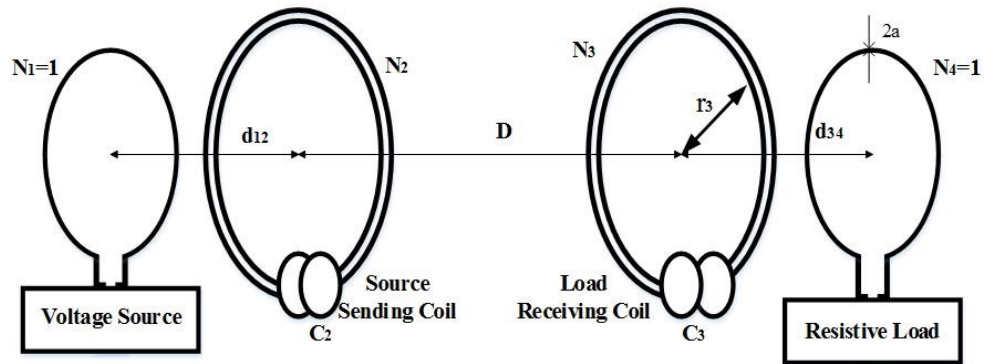
Figure 4-1: Indirect resonant wireless power transfer system.

Given the minimum load rating and the distance range between the sending and receiving resonant coils (D), the design objective is to find the proper wire and coil diameters, as well as the distances between the loops and the coils. It is assumed that the coils are of circular shape. In addition, it is assumed that the source and load loops (loops 1 and 4) are of the same shape and dimension. The sending and receiving coils (coils 2 and 3) are also identical and the material used for all the loops and coils are identical and have the same radii.

The design problem can be defined like an optimization problem with some differences. The desired goal for this problem is smaller size, which is interpreted into smaller radii in the coils. The constraints for the design problem are listed below:

1) The maximum number of turns (N_i) is limited to N_{max}

2) The capacitors' capacities are limited to ($C_{i,max}$)

3) Wires' diameter (2a) has a limited number of choices

4) A minimum power (P_{min}) is transferred to the load for all distances D in the range (D_{min}- D_{max})

5) The operating frequency is bound to f_{max}

The first three constraints are direct limitations to be considered in the design, while the rest of the constraints become feasible under certain operating frequency and depend on the operating status of the WPT system with the load and the source. The former are named static constraints and the latter are named operating constraints.

It is important to find a relationship between the circuit elements' dimensions and the equivalent circuit model parameters (L, R, C and M).

For one single coil, the total resistance R and self-inductance L of the coil are calculated as [62]:

$$L = r \mu_0 \mu_r N^2 \left[\ln\left(\frac{8r}{a}\right) - 2 \right] \qquad \text{Eq. 4-1}$$

$$R_o = \frac{N.r}{a} \sqrt{\frac{2 \pi f \mu_0 \mu_r}{2 \sigma}} \qquad \text{Eq. 4-2}$$

$$R_r = 20N\left(\left(\frac{2 \pi f}{c}\right) \pi r^2\right)^2 \qquad \text{Eq. 4-3}$$

$$R = R_o + R_r \qquad \text{Eq. 4-4}$$

In equations Eq. 4-1 to Eq. 4-4, L is the self-inductance of the coil; N is the turns ratio in the coil; r is the coil radius; a is the wire radius; f is the operating frequency; σ is the conductivity coefficient; c is light speed. R_r and R_o are radiative and ohmic resistances respectively, which add up to form the whole coil resistance.

In each coil, a capacitor is added to provide resonance with the fixed frequency, which is the same as the maximum achievable frequency (f_{max}). Hence, the coils include a capacitor with the value of Eq. 4-5.

$$C = \frac{1}{(2 \pi f_r)^2 L}$$

<div align="right">Eq. 4-5</div>

Also, the mutual inductance of each two coils can be calculated with Neumann formula (Eq. 4-6) [60].

$$M_{12} = \frac{\mu_0 \sqrt{r_1 r_2 \beta}}{4\pi} \int_0^{2\pi} \int_0^{2\pi} \frac{\cos(\varphi_a - \varphi_b) d\varphi_a d\varphi_b}{\sqrt{1 - 2\beta . \cos(\varphi_a - \varphi_b)}}$$

<div align="right">Eq. 4-6</div>

Where β is obtained from (Eq. 4-7).

$$\beta = \frac{r_1 r_2}{D^2 + r_1^2 + r_2^2}$$

<div align="right">Eq. 4-7</div>

Using Taylor's series across zero for the term φ_a-φ_b, Eq. 4-6 can be simplified to Eq. 4-8.

$$M_{12} = \frac{\mu_0 \sqrt{r_1 r_2 \beta}}{4 \pi} [2 \beta \pi^2 + \frac{15}{4} \beta^3 \pi^2 + \frac{315}{32} \beta^5 \pi^2 + \frac{56199}{2048} \beta^7 \pi^2]$$

<div align="right">Eq. 4-8</div>

Eq. 4-8 is a closed form and the greater the distance D, the smaller the value of β, hence the more precise the formula will be. β is the largest when r_1 and r_2 are equal and D is minimum, which means β is always smaller than 0.5. So, ignoring the higher terms in Eq. 4-8 is reasonable when the distance D is in the range of the radii of the coils or larger.

4.3   Circuit analysis

The design problem is dependent on the operating condition of the system. The two parameters, output power and efficiency, can determine the performance. The distance between the coils (D) as well as the optimal operating frequency (f_{op}) selection, can both change the performance of a given possible design drastically. Given the circuit model (Figure 4-2) for indirect-fed WPT [19], the output power of the WPT system can be calculated as Eq. 4-9.
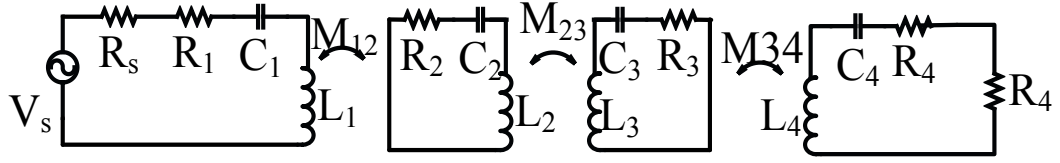
Figure 4-2: The circuit model of the indirect-fed WPT system.

$$P_{out}=\frac{R_L\,\omega^6 M_{12}^2 M_{23}^2 M_{34}^2 |V_i|^2}{2\left[R_L+\dfrac{M_{12}^2 M_{34}^2\,\omega^4+Z_3Z_4M_{12}^2\,\omega^2+Z_sZ_4M_{23}^2\,\omega^2+Z_sZ_2M_{34}^2\,\omega^2+Z_sZ_2Z_3Z_4}{A}\right]^2 A^2}$$
Eq. 4-9

The values of Z_1, Z_2, Z_3, Z_4, Z_s and A are shown in Eq. 4-10 - Eq. 4-15.

$$Z_1=R_1+j\,\omega\,L_1+\frac{1}{j\,\omega\,C_1}$$
Eq. 4-10

$$Z_2=R_2+j\,\omega\,L_2+\frac{1}{j\,\omega\,C_2}$$
Eq. 4-11

$$Z_3=R_3+j\,\omega\,L_3+\frac{1}{j\,\omega\,C_3}$$
Eq. 4-12

$$Z_4=R_4+j\,\omega\,L_4+\frac{1}{j\,\omega\,C_4}$$
Eq. 4-13

$$Z_s=Z_1+R_s$$
Eq. 4-14

$$A=Z_3M_{12}^2\,\omega^2+Z_sM_{23}^2\,\omega^2+Z_2Z_3Z_s$$
Eq. 4-15

The design problem might be able to deliver more power in an operating frequency different from resonance frequency. Hence, the operating constraint for output power is done for the best frequency (the one which gives the highest output power) below the resonant frequency.

4.3.1   Analysis of a given design

According to Eq. 4-9, at the fixed resonance frequency (f_r), while changing the distance D results in a bell-shape curve; i.e. starting from very close distance (minimum D), the output power increases with D until a critical point D_{cr} (which corresponds to a critical M_{cr}). However, further increase in D causes the output power to decrease. For the distances below D_{cr}, which will be called overcoupled area, working in an operating frequency (f_{op}) different from f_r helps meet higher output powers. This fact is shown in Fig. 3 in the simulation section. In other words, given any distance in the overcoupled range, there exists two frequencies, different from f_r, in which the output power is locally maximum. This is rather close to the concept of frequency splitting discussed in the literature [14] and [9], with the difference that this new concept is about the output power.

For a given design, output power is always decreasing if the proper frequency is chosen. Hence, if the voltage source is capable of providing any frequency, it is expected that the bottleneck for the 4th constraint is when the coils are at their farthest position, i.e. maximum D.

4.3.2   Sensitivity Analysis of the design

Substituting Eq. 4-8 and Eq. 4-1 in Eq. 4-9, a direct analytical function that relates output power to the distance D is achieved. Taking the derivative of Eq. 4-9 with respect to r_3 proves Eq. 4-16.

$$\frac{\partial P_{out}}{\partial r_3} > 0 \qquad\qquad\qquad \text{Eq. 4-16}$$

The interpretation of Eq. 4-16 is that when other parameters remain unchanged, the larger the diameter of the sending and receiving coils are, the larger the amount of output power will become; i.e. the trade-off for the design problem is coil size versus output

power. If the design requirements need higher output power rating, an increase in the sending and receiving coil radii helps.

When constant output power is needed (rather than a minimum output power), the critical (knee) point should be determined. The knee point is on the output power curve at resonant frequency [11]. At the knee point, the derivative of output power with respect to M_{23} is zero. By keeping all other parameters constant, M_{23} at the knee point (M_{cr}) is calculated in Eq. 4-17.

$$\frac{\partial P_{out}}{\partial M_{23}}=0 \Rightarrow M_{23}=\frac{\omega\, M_{12}M_{34}}{\sqrt{R_L R_s}} \qquad \text{Eq. 4-17}$$

To derive Eq. 4-17, Eq. 4-9is rewritten at the resonant frequency as inEq. 4-18.

$$Z_i=R_i \qquad \text{Eq. 4-18}$$

$$P_{out}=\frac{R_L M_{12}^2 M_{34}^2\, \omega^{\,2}}{2} \cdot \frac{M_{23}^2}{\left(M_{12}^2 M_{34}^2\, \omega^{\,2}+R_L R_s M_{23}^2\right)^2} \qquad \text{Eq. 4-19}$$

As shown in Eq. 4-18, the model becomes simpler at resonant frequency. The derivative of Eq. 4-19 with respect to the main coils' mutual inductance, is obtained as in Eq. 4-20.

$$\frac{dP_{out}}{d(M_{23}^2)}=\frac{R_L M_{12}^2 M_{34}^2\, \omega^{\,2}}{2} \cdot \frac{\left(M_{12}^2 M_{34}^2\, \omega^{\,2}\right)^2-\left(R_L R_s M_{23}^2\right)^2}{\left(M_{12}^2 M_{34}^2\, \omega^{\,2}+R_L R_s M_{23}^2\right)^2} \qquad \text{Eq. 4-20}$$

According to Eq. 4-17, critical distance (D_{cr}) is a point that has constant M_{23} if the frequency, M_{12} and M_{34} are fixed. Because M_{23} is constant, and it is known that M_{23} decreases with D, hence: by increasing the radius of the coils, D_{cr} also increases. In other words, the knee point of the output power versus distance curve will be at larger distances.

Setting Eq. 4-20 to zero, only leads to one point which is derived in Eq. 4-17. Based on Eq. 4-20, this point is a maximum point, because at values of M_{23} lower than Eq. 4-17, the derivative is positive and at values higher than Eq. 4-17, the derivative is negative.

4.4   Algorithm to find the optimal size

In terms of maximum output power, there is an optimal frequency for each distance. Hence, if the voltage source is capable of providing any frequency, the bottleneck of the 4th constraint in 4.2 is when the coils are at their farthest position, i.e. at D_{max}. Based on this, the flowchart in Figure 4-3 is proposed. In Figure 4-3, the minimum radius of the sending and receiving coils is determined so that a minimum output power ($P_{desired}$) is satisfied. The algorithm is a smart try and error on the coils' radius. The radius is increased/decreased slightly so as to keep the output power above the desired level. The solution is the minimum radius that satisfies $P_{out} > P_{desired}$ at D_{max}. This flowchart is useful when the parameters for the rest of the RWPT system are determined, e.g. loop 1 and loop 4 sizes.

4.5   Case Study

The desired design discussed in the previous sections is done for a 15 W load. The distance range is 40-80 cm from the sending resonant coil to the receiving resonant coil. In other words, it is needed for the WPT to transfer a minimum output power of 15 W for all values of D in the range of 40-80 cm. The resonance frequency is set to 100 kHz. The operating frequency can be varied from 95 kHz to 100 kHz. Table 4-1 shows the options for optimization variables which form a total of 28800 set of options.
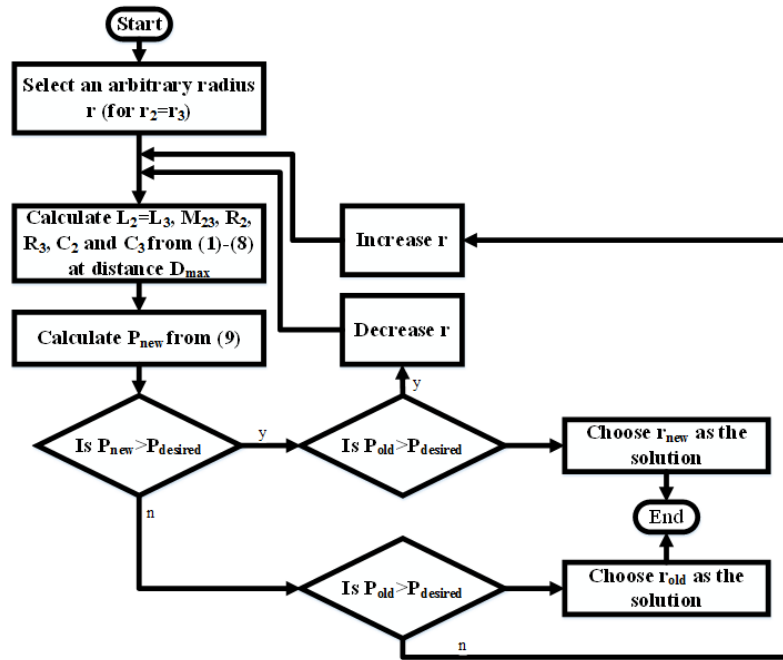
Figure 4-3: Flowchart to determine the radius of sending and receiving coils.

The results show that the minimum size of the receiving package with the given constraints, is achieved by the values given in Table 4-2. The important result is that the optimal solution occurs when the coils' and loops' diameters are equal.

Table 4-1: Optimization variables' options

Optimization Variable	Options
r_2 & r_3	[0.05 -0.50] meters
r_1 & r_4	[0.05 -0.50] meters
N_2 & N_3	[1-10] turns
a	[3.6740 , 3.2720 , 2.9135 , 2.5945 , 2.3105 , 2.0575 , 1.8325 , 1.6320 , 1.4530 , 1.2940] millimetres Wires #1 to #10 respectively [63]
d_{12} and d_{34}	[1 , 2 , 5 , 10 , 20, 50] centimeters

Table 4-2:Dimensions in the solution design.

Optimization Variable	Solution
r_2 & r_3	0.075 meters
r_1 & r_4	0.075 meters
N_2 & N_3	10 turns
A	3.6740 mm (Wire #1)
d_{12} and d_{34}	1 centimeter

Figure 4-4 shows the output power of the WPT with respect to D. As r_2 and r_3 are small and approximately in the same range as D (or smaller), Eq. 4-8 can be used with error less than 0.1%. Eq. 4-9 and Eq. 4-17 can explain why Figure 4-4 has an asymptote at infinity and a maximum at D_{cr}.
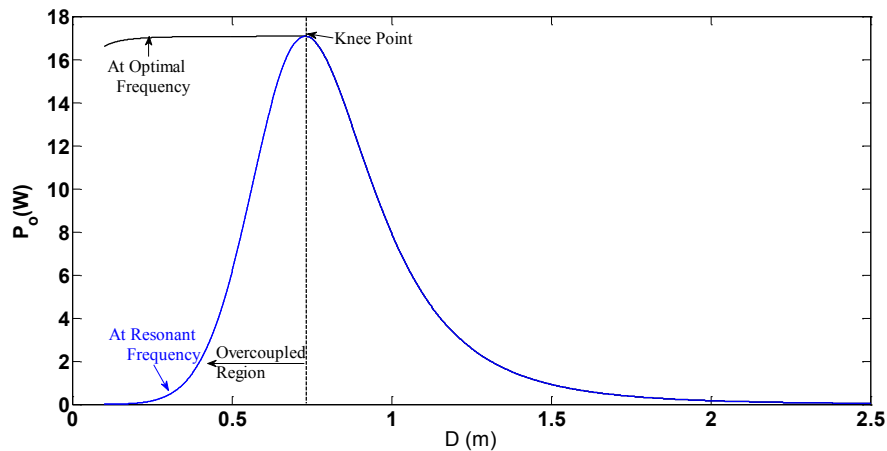
Figure 4-4: Output power versus distance for the optimal design

Figure 4-4 shows that for the optimal design, the critical distance (D_{cr}) is 0.729 m. Moreover, using the flowchart in Fig. 3, it is concluded that, the critical r_3 (=r_2) is 7.2 cm that occurs at D=80 cm where 15 W can be delivered to R_L. It can also be concluded from Figure 4-4 that the output power is low at resonant frequency in the overcoupled region.

However, by controlling the source frequency, the output power can be kept almost at a constant curve above 15 W.

As shown in Section III, the output power increases with the coil size. Figure 4-5 shows the sensitivity analysis of the output power delivered to the load with respect to the coil radius, for all the distances in range 0.4-0.8 m.

It can be concluded that the feasible designs (the ones that can satisfy the power delivery constraint) are the ones that can satisfy the condition only at D_{max}. In other words, satisfying the power condition at D=0.8 m is a sufficient condition for the general case of satisfying minimum power (15W) in the range of 0.4-0.8 m. It can also be concluded from Figure 4-5 that if the distance range decreases, the optimal design can be realized with smaller sizes. For example, coils of 6cm radius can satisfy the minimum power of 15W in the range 0.4-0.65 m.
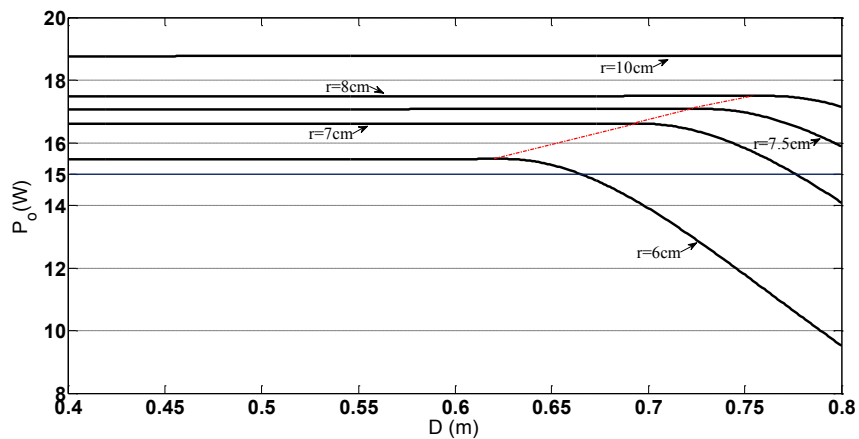
Figure 4-5: Sensitivity analysis on the radius of the coil

In Figure 4-5, the conclusions in section 4.3 are illustrated: an increase in the radius of the coils cause the knee point to move to a farther distance. The knee points are

connected via the dash-dotted red line in Figure 4-5. On the dash-dotted red line, all the points have the same M_{23}, albeit at different r and D values.

As shown in 4.3, the output power increases with an increase in the coil size (radius). Same concept does exist for the maximum output power. Figure 4-6 is derived by changing all the four elements' radii equally while other parameters are constant. It is observed that increasing the distance between the sending coil and sending loop (equally between receiving coil and receiving loop) has a negative effect on output power. It is also observed that the maximum output power increases with a radius increase. However, this would not be the case if the radii of r_1 and r_4 are kept constant (5 centimeters). The graph in this case is shown in Figure 4-7. It is observed that the maximum output power does not monotonically increase with respect to r_2 and r_3. This is why the assumption of equal size for all the coils is a good one.
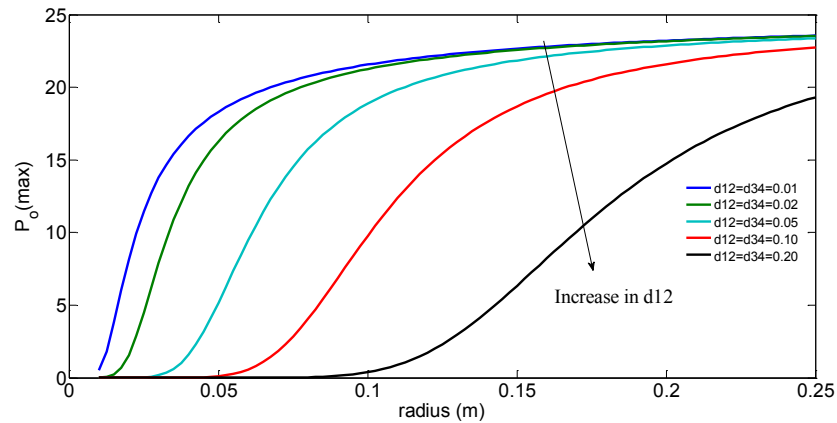
Figure 4-6: Maximum Output power (W) when all radii are equal at different values of d_{12}
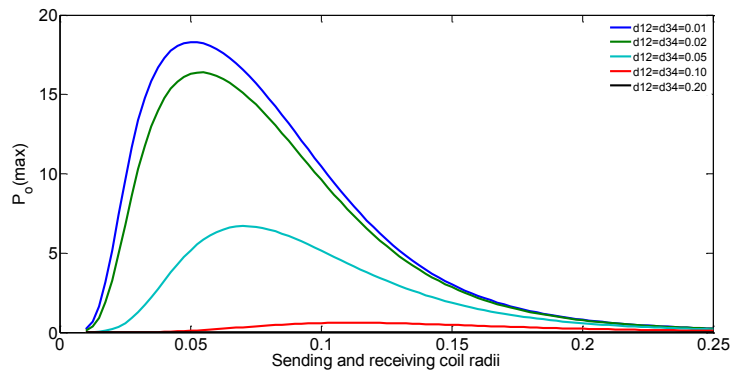
Figure 4-7: Maximum Output power when radii of r_1 and r_4 are kept constant for different values of d_{12}

4.6   Conclusion

In this chapter, a design approach for an indirect-fed type resonant wireless power transfer system is proposed. The objective of the design procedure is to find a minimum structure size. The relations between the dimensions of the coils and their positioning is first translated into a circuit model and then to the output power. It is concluded that the optimal design for a range of distances between the sending and receiving coils, is better achieved by controlling the operating frequency according to the distance. Moreover, the bottleneck of the design constraints is to satisfy the minimum power condition at the maximum distance in the desired distance range. A flowchart is provided to find an optimum solution. All optimal solutions are common in having equal diameters for all coils. The simulations results to find a 15W WPT system is presented to validate the analytical results. For further study, a more precise model for circuit analysis, which considers the mutual inductance between the non-adjacent coils, is suggested.

CHAPTER 5

CONCLUSION AND FUTURE WORK

Wireless power in power electronics has been applied to charge electric vehicles and applications where using wires is unsafe or undesired. Applications range from a few Watts to several kilowatts. For these applications, two or more coils are involved, and the energy transfer is through magnetic coupling of these coils. Existing magnetic design for such applications was reviewed in this thesis and then simple magnetic design procedure was proposed for the chosen topology's control and magnetic design.

Converter topologies in the literature was reviewed. Converters are needed to make the voltage level and specifically frequency level possible. Detailed process of designing a converter and a new control method applicable to high frequency was developed in this thesis. The proposed converter and control system offer a new method to control the WPT system so that the frequency is automatically determined to guarantee ZVS. Both IPT and RWPT approaches were studied in this thesis with more weight given to the IPT system for implementation. The conclusions of the IPT design are listed below.

    i.   The control method achieves power control and soft switching with two control loops. This method reduces calculations burden in every sampling cycle.

ii.   Biggest challenge in building the experimental setup is sampling frequency. The problem was addressed by multi-rate control approach by dividing the control process into high frequency and medium frequency sections.

iii.   The important contribution of RWPT design was to determine the design bottleneck. The bottleneck is to guarantee the maximum required power of the load at the maximum distance.

5.1   Suggested Future Work:

The tasks below are suggested for future work.

i.   Development of a fixed power load model; most power appliances necessitate a certain level of power.

ii.   Implementation of the resonant wireless power transfer system introduced in chapter 5.

iii.   Extending the control method to variable distance position for the coils

iv.   Analyze the effect of misalignment on the control method

BIBLIOGRAPHY

[1]   K. Y. Kim, Ed., *Wireless Power Transfer- Principles and engineering explorations*. InTech, 2012.

[2]   A. Kurs, A. Karalis, R. Moffatt, J. D. Joannopoulos, P. Fisher, and M. Soljacic, "Wireless power transfer via strongly coupled magnetic resonances.," *Science*, vol. 317, no. 5834, pp. 83–6, 06-Jul-2007.

[3]   Y. Zhang, Z. Zhao, and K. Chen, "Frequency Decrease Analysis of Resonant Wireless Power Transfer," *IEEE Trans. Power Electron.*, vol. 29, no. 3, pp. 1058–1063, Mar. 2014.

[4]   D. Arnitz and M. S. Reynolds, "Multitransmitter Wireless Power Transfer Optimization for Backscatter RFID Transponders," *IEEE Antennas Wirel. Propag. Lett.*, vol. 12, pp. 849–852, 2013.

[5]   O. Qasaimeh, W. Zhou, and P. Bhattacharya, "Monolithically Integrated Low-Power Phototransceivers for Optoelectronic Parallel Sensing and Processing Applications," vol. 19, no. 4, pp. 546–552, 2001.

[6]   D. a. J. Pearce and D. Grace, "Optimum antenna configurations for millimetre-wave communications from high-altitude platforms," *IET Commun.*, vol. 1, no. 3, pp. 359–364, 2007.

[7]   D. C. Ludois, J. K. Reed, S. Member, and K. Hanson, "Capacitive Power Transfer for Rotor Field Current in Synchronous Machines," *IEEE Trans. Power Electron.*,

vol. 27, no. 11, pp. 4638–4645, 2012.

[8]   J. Dai and D. C. Ludois, "Single active switch power electronics for kilowatt scale

capacitive power transfer," *IEEE J. Emerg. Sel. Top. Power Electron.*, vol. 3, no.

1, pp. 315–323, 2015.

[9]   S. Y. R. Hui, W. Zhong, and C. K. Lee, "A Critical Review of Recent Progress in

Mid-Range Wireless Power Transfer," *IEEE Trans. Power Electron.*, vol. 29, no.

9, pp. 4500–4511, Sep. 2014.

[10]   C. Huang, J. T. Boys, and G. A. Covic, "LCL Pickup Circulating Current

Controller for Inductive Power Transfer Systems," *IEEE Trans. Power Electron.*,

vol. 28, no. 4, pp. 2081–2093, 2013.

[11]   "Noise Suppression Methods in Qi Standard Wireless Chargers," *Murata

application note*, 2013. [Online]. Available:

http://www.murata.com/about/newsroom/techmag/metamorphosis18/appnote/02.

[12]   Hua Bai; Chris Mi, "Power electronics in electric vehicles," in *Transients of

Modern Power Electronics*, 2010.

[13]   W. X. Zhong and S. Y. Hui, "Wireless power domino-resonator systems with

noncoaxial axes and circular structures," *IEEE Trans. Power Electron.*, vol. 27, no.

11, pp. 4750–4762, Nov. 2012.

[14]   H. Hirayama, "Equivalent Circuit and Calculation of Its Parameters of Magnetic-

Coupled-Resonant Wireless Power Transfer."

[15]   M. Pinuela, S. Member, D. C. Yates, S. Lucyszyn, S. Member, and P. D.

Mitcheson, "Maximizing DC-to-Load Efficiency for Inductive Power Transfer,"

IEEE Trans. Power Electron., vol. 28, no. 5, pp. 2437–2447, 2013.

[16] M. Budhia, G. a. Covic, and J. T. Boys, "Design and optimization of circular magnetic structures for lumped inductive power transfer systems," *IEEE Trans. Power Electron.*, vol. 26, no. 11, pp. 3096–3108, 2011.

[17] N. Tesla, "Apparatus for transmitting electrical energy," 1119732, 1914.

[18] V. Pala, H. Peng, P. Wright, M. M. Hella, and T. P. Chow, "Integrated High-Frequency Power Converters Based on GaAs pHEMT : Technology Characterization and Design Examples," *IEEE Trans. Power Electron.*, vol. 27, no. 5, pp. 2644–2656, 2012.

[19] A. P. Sample, D. A. Meyer, and J. R. Smith, "Analysis , Experimental Results , and Range Adaptation of Magnetically Coupled Resonators for Wireless Power Transfer," *IEEE Trans. Ind. Electron.*, vol. 58, no. 2, pp. 544–554, 2011.

[20] M. Budhia and J. Boys, "Development of a single-sided flux magnetic coupler for electric vehicle IPT charging systems," *… , IEEE Trans.*, vol. 60, no. 1, pp. 318–328, 2013.

[21] G. a. Covic, J. T. Boys, M. L. G. Kissin, and H. G. Lu, "A three-phase inductive power transfer system for roadway-powered vehicles," *IEEE Trans. Ind. Electron.*, vol. 54, no. 6, pp. 3370–3378, 2007.

[22] J. T. Boys and G. A. Covic, "Inductive power transfer systems (IPT) Fact Sheet: No . 1 – Basic Concepts," *Https://Www.Qualcomm.Com/Documents/Inductive-Power-Transfer-Systems-Ipt-Fact-Sheet-No-1-Basic-Concepts*, no. 1, 2013.

[23] S. Aldhaher, P. C. Luk, S. Member, K. El, K. Drissi, and J. F. Whidborne, "High-Input-Voltage High-Frequency Class E Rectifiers for Resonant Inductive Links," *IEEE Trans. Power Electron.*, vol. 30, no. 3, pp. 1328–1335, 2015.

[24] S. Birca-Galateanu and A. Ivas, "Class E Low dv = dt and Low di = dt Rectifiers : Energy Transfer , Comparison , Compact Relationships," *IEEE Trans. Circuits Syst.*, vol. 48, no. 9, pp. 1065–1074, 2001.

[25] J. Hu, A. D. Sagneri, J. M. Rivas, Y. Han, S. M. Davis, D. J. Perreault, and S. Member, "High-Frequency Resonant SEPIC Converter With Wide Input and Output Voltage Ranges," *IEEE Trans. Power Electron.*, vol. 27, no. 1, pp. 189–200, 2012.

[26] H. L. Li, A. P. Hu, and G. A. Covic, "A direct AC-AC converter for inductive power-transfer systems," *IEEE Trans. Power Electron.*, vol. 27, no. 2, pp. 661–668, 2012.

[27] "Wireless energy transfer converters," 8497601.

[28] J. . T. Boys, A. P. Hu, and G. A. Covic, "Critical Q analysis of a current-fed resonant converter for ICPT applications," *Electron. Lett.*, vol. 36, no. 17, pp. 1440–1442, 2000.

[29] R. L. Steigerwald, "A comparison of half-bridge resonant converter topologies," *IEEE Trans. Power Electron.*, vol. 3, no. 2, pp. 174–182, Apr. 1988.

[30] J.-H. Choi, S.-K. Yeo, J.-S. Lee, and G.-H. Cho, "Resonant Regulating Rectifiers (3R) Operating for 6.78 MHz Resonant Wireless Power Transfer (RWPT)," *IEEE Trans. Solid-State Circuits*, vol. 48, no. 12, pp. 2989–3001, 2013.

[31] J.-Y. Lee and B.-M. Han, "A Bidirectional Wireless Power Transfer EV Charger Using Self-Resonant PWM," *IEEE Trans. Power Electron.*, vol. 30, no. 4, pp. 1784–1787, Apr. 2015.

[32] R. Beiranvand, B. Rashidian, M. R. Zolghadri, and S. M. H. Alavi, "Using LLC

Resonant Converter for Designing Wide-Range Voltage Source," *IEEE Trans. Ind. Electron.*, vol. 58, no. 5, pp. 1746–1756, 2011.

[33] C. S. Wang, G. a. Covic, and O. H. Stielau, "Investigating an LCL load resonant inverter for inductive power transfer applications," *IEEE Trans. Power Electron.*, vol. 19, no. 4, pp. 995–1002, 2004.

[34] T. Nagashima, X. Wei, E. Bou, S. Member, E. Alarcón, S. Member, and M. K. Kazimierczuk, "Analysis and Design of Loosely Inductive Coupled Wireless Power Transfer System Based on Class- DC-DC Converter for Efficiency Enhancement," vol. 62, no. 11, pp. 2781–2791, 2015.

[35] K. Woronowicz, A. Safaee, and T. Dickson, "Single-phase Zero Reactive Power Wireless Power Transfer Topologies Based on Boucherot Bridge Circuit Concept," 2016.

[36] "Tesla Coil." [Online]. Available: http://coil32.net/online-calculators/flat-spiral-pancake-tesla-coil.html.

[37] M. T. Thompson, "Inductance Calculation Techniques --- Part II : Approximations and Handbook Methods," in *Power Control and Intelligent Motion*, 1999, no. December, pp. 1–11.

[38] Y. Cheng and Y. Shu, "A New Analytical Calculation of the Mutual Inductance of the Coaxial Spiral Rectangular Coils," *IEEE Trans. Magn.*, vol. 50, no. 4, 2014.

[39] B. Fahimi and M. McDonough, "Comparison between circular and square coils for use in Wireless Power Transmission," *9th IET Int. Conf. Comput. Electromagn. (CEM 2014)*, no. 9, p. 5.14-5.14, 2014.

[40] J. J. Casanova, Z. N. Low, and J. Lin, "A loosely coupled planar wireless power

system for multiple receivers," *IEEE Trans. Ind. Electron.*, vol. 56, no. 8, pp. 3060–3068, 2009.

[41]   J. T. Boys, G. A. Covic, and R. P. Development, "IPT Fact Sheet Series : No . 2 Magnetic Circuits for Powering Electric Vehicles," no. 2.

[42]   R. Bosshard, U. Badstubner, J. W. Kolar, and I. Stevanovic, "Comparative evaluation of control methods for Inductive Power Transfer," *2012 Int. Conf. Renew. Energy Res. Appl.*, vol. 1, no. 1, pp. 1–6, 2012.

[43]   A. Witulski and R. Erickson, "Design of the Series Resonant Converter for Minimum Component Stress," *Aerosp. Electron. Syst.*, vol. 22, no. 4, pp. 1–8, 1986.

[44]   H. Pinheiro and P. K. Jain, "Analysis & Modeling of a Self-sustained Oscillation Series-Parallel Resonant Converter with Capacitive Output Filter Using Sampled-Data Analytical Technique," pp. 282–289, 2003.

[45]   M. Z. Youssef and P. K. Jain, "Series-Parallel Resonant Converter in Self-Sustained Oscillation Mode With the High-Frequency Transformer-Leakage-Inductance Effect: Analysis, Modeling, and Design," *IEEE Trans. Ind. Electron.*, vol. 54, no. 3, pp. 1329–1341, 2007.

[46]   K. Woronowicz, A. Safaee, and T. Dickson, "Single-Phase Zero Reactive Power Wireless Power Transfer Topologies Based on Boucherot Bridge Circuit Concept," *Can. J. Electr. Comput. Eng.*, vol. 38, pp. 323–337, 2015.

[47]   R. Bosshard, J. Muhlethaler, J. W. Kolar, and I. Stevanovic, "The n-a-Pareto front of inductive power transfer coils," *IECON 2012 - 38th Annu. Conf. IEEE Ind. Electron. Soc.*, pp. 4270–4277, 2012.

[48]   R. Bosshard, S. Member, J. W. Kolar, J. Mühlethaler, S. Member, and B. Wunsch, "Power Transfer Coils for Electric Vehicles," vol. 3, no. 1, pp. 50–64, 2015.

[49]   R. Bosshard and U. Badstubner, "Comparative evaluation of control methods for inductive power transfer," … *Energy Res. …*, vol. 1, no. Icrera, 2012.

[50]   A. Pevere and R. Petrella, "Design of a high efficiency 22 kW wireless power transfer system for EVs fast contactless charging stations."

[51]   H. Sakamoto, H. Harada, and Y. Matsuda, "Self Oscillated PWM Converter with Impulse Resonant Soft-switching," pp. 340–343, 2003.

[52]   J. Sallan, J. L. Villa, a. Llombart, and J. F. Sanz, "Optimal Design of ICPT Systems Applied to Electric Vehicle Battery Charge," *IEEE Trans. Ind. Electron.*, vol. 56, no. 6, pp. 2140–2149, 2009.

[53]   D. a. Stricker, G. P. Alba, C. C. Anderson, D. D. Bing, R. W. Bland, S. C. Dickson, T. G. Dignan, P. Gagnon, R. T. Johnson, and C. M. Seneclauze, "Characteristics of high-transmission-probability tunnel junctions for use as particle detectors," *IEEE Trans. Magn.*, vol. 25, no. 2, pp. 1343–1346, 1989.

[54]   H.-M. Hsu, "Analytical formula for inductance of metal of various widths in spiral inductors," *Signal Processing*, vol. 51, no. 8, pp. 1343–1346, 2004.

[55]   E. Ashoori, F. Asgarian, A. M. Sodagar, and E. Yoon, "Design of double layer printed spiral coils for wirelessly-powered biomedical implants," *Proc. Annu. Int. Conf. IEEE Eng. Med. Biol. Soc. EMBS*, pp. 2882–2885, 2011.

[56]   D. K. Cheng, *Fundamentals of Engineering Electromagnetics*, 2nd ed. Pearson, 1992.

[57]   C. Paul, *Inductance, Loop and Partial*. Wiley, 1994.

[58] Z. Zhang, K. T. Chau, C. Qiu, C. Liu, and S. Member, "Energy Encryption for Wireless Power Transfer," vol. 8993, no. c, pp. 1–10, 2014.

[59] S. Cheon, Y.-H. Kim, S.-Y. Kang, M. L. Lee, J.-M. Lee, and T. Zyung, "Circuit-Model-Based Analysis of a Wireless Energy-Transfer System via Coupled Magnetic Resonances," *IEEE Trans. Ind. Electron.*, vol. 58, no. 7, pp. 2906–2914, Jul. 2011.

[60] T. Imura and Y. Hori, "Maximizing air gap and efficiency of magnetic resonant coupling for wireless power transfer using equivalent circuit and Neumann formula," *IEEE Trans. Ind. Electron.*, vol. 58, pp. 4746–4752, 2011.

[61] J. Shin, S. Shin, Y. Kim, S. Ahn, S. Lee, G. Jung, S. J. Jeon, and D. H. Cho, "Design and implementation of shaped magnetic-resonance-based wireless power transfer system for roadway-powered moving electric vehicles," *IEEE Trans. Ind. Electron.*, vol. 61, pp. 1179–1192, 2014.

[62] H.-C. Son, J.-W. Kim, Y.-J. Park, and K.-H. Kim, "Efficiency analysis and optimal design of a circular loop resonant coil for wireless power transfer," in *2010 Asia-Pacific Microwave Conference*, 2010, no. L, pp. 849–852.

[63] W. Stutzman and G. Thiele, *Antenna Theory and Design*. Wiley, 1998.